# Accuracy of first-principles interatomic interactions and predictions of ferroelectric phase transitions in perovskite oxides: Energy functional and effective Hamiltonian

Arpita Paul, Jianwei Sun, John P. Perdew, and Umesh V. Waghmare

Phys. Rev. B **95**, 054111 — Published 15 February 2017

DOI: 10.1103/PhysRevB.95.054111

# Accuracy of first-principles interatomic interactions and predictions of ferroelectric phase transitions in perovskite oxides: energy functional and effective Hamiltonian

Arpita Paul,[1] Jianwei Sun,[2] John P. Perdew,[3, 4] and Umesh V. Waghmare[1, *]

[1] *Theoretical Sciences Unit, Jawaharlal Nehru Centre for*
*Advanced Scientific Research, Jakkur, Bangalore 560 064, India*
[2] *Department of Physics, The University of Texas at El Paso, El Paso, TX 79968, USA*
[3] *Department of Physics, Temple University,*
*1925 N. 12th St., Philadelphia, PA 19122, USA*
[4] *Department of Chemistry, Temple University,*
*1901 N. 13th St., Philadelphia, PA 19122, USA*

(Dated: January 19, 2017)

## Abstract

While first-principles density functional theory (DFT) based models have been effective in capturing the physics of ferroelectric phase transitions in $BaTiO_3$, $PbTiO_3$ and $KNbO_3$, quantitative estimates of the transition temperatures ($T_C$'s) suffer from errors that are believed to originate from the errors in estimating lattice constants obtained within local density (LDA) and gradient density (GGA) approximations of DFT. The recently-developed strongly constrained and appropriately normed (SCAN) meta-GGA functional has been shown to be quite accurate in estimation of lattice constants. Here, we present a quantitative analysis of the estimates of ferroelectric ground state properties of eight perovskite oxides and transition temperatures of $BaTiO_3$, $PbTiO_3$ and $KNbO_3$ obtained with molecular dynamics (MD) simulations using an effective Hamiltonian derived from the SCAN meta-GGA based DFT. Relative to LDA, we find an improvement in estimates of $T_C$'s, which arises from the changes in calculated strain-phonon, anharmonic coupling constants and strength of ferroelectric instabilities, i.e., frequencies of the soft modes. We also assess the errors in $T_C$ originating from approximately integrating out the high-energy phonons during construction of the model Hamiltonian through estimates of the effects of fourth-order couplings between soft mode and higher energy modes of $BaTiO_3$, $PbTiO_3$ and $KNbO_3$. We find that inclusion of these anharmonic couplings results in deeper double-well energy functions of ferroelectric distortions and further improvement in the estimates of transition temperatures. Consistently improved estimates of lattice constants and transition temperatures with the SCAN meta-GGA calculations augur well for their use in simulations of superlattices or hetero-structures of perovskite oxides, in which the effects of lattice matching are critical.

## I. INTRODUCTION

Ferroelectrics are an important class of materials that exhibit a spontaneous macroscopic electric polarization that is switchable with application of an electric field, and hence have a wide range of technological applications[1,2]. Perovskite oxides are the most interesting of ferroelectric materials, and have been studied frequently[3,4] since the discovery of barium titanate in 1945[5]. Perovskite oxides have a chemical formula $ABO_3$, with the A cation at the corner of the cube, and with the B and O atoms located at the body-centered and face-centered positions respectively. There is a remarkable diversity in the structural instabilities and phase transitions that these perovskites undergo: ferroelectric transitions (associated with polar distortion) in $BaTiO_3$, $PbTiO_3$ and $KNbO_3$, antiferroelectric transition (involving nonpolar distortion) in $PbZrO_3$ and antiferrodistortive transition (associated with tilting of oxygen octahedra) in $SrTiO_3$[4,6]. These phase transitions and competing instabilities have singularly important consequences to their properties relevant to technological applications. First-principles density functional calculations have been used extensively in microscopic studies of structural transitions via identifying the responsible phonon mode for structural transition, studying the stability of the intermediate phases and predicting transition temperatures ($T_C$)[4,7–9]. It has been established that harmonic and anharmonic couplings between phonons and strain-phonon coupling constants are the most crucial parameters that govern the phase transitions in perovskites[4,8,10]. Accuracy in determination of these parameters and subsequent estimation of transition temperatures is naturally limited by the DFT errors in estimation of lattice constants.

Earlier all-electron calculations (FLAPW) within the local density approximation (LDA) predicted the cubic phases of $KNbO_3$ to be stable (in contradiction to experimental results), and $PbTiO_3$ and $BaTiO_3$ to be unstable at the optimized lattice constant[4,11]. The discrepancies between experimental and theoretical results (using LDA) for cubic $KNbO_3$ have been removed by implementing ultrasoft pseudopotentials[4]. But, LDA is well known to underestimate the lattice constant by 1-2% as it neglects the effects of inhomogeneity in electron density[4,12]. Such over-binding of the structure predicted within LDA results in underestimation of the difference in energies of cubic and distorted structures[13]. This is because the ferroelectric instability is a strong function of cell volume of those materials[13,14].

While *ab initio* MD or MC simulations would be effective in estimation of the temperature-dependent transition properties, the size (length scale) of a system needed to capture the phase transition and corresponding computational cost make them presently impractical. Instead, an approximate approach is adopted that uses an effective Hamiltonian, which focuses on the low-energy structural configurations in MD or MC simulations[7,8]. Thus, there are two sources of errors in first-principles description of ferroelectric transitions: (a) ones arising from the choice of DFT functional, and (b) ones arising from the truncation of the set of configurations through the effective Hamiltonian.

As an example, the too-shallow potential well in $BaTiO_3$ underestimates the transition temperature ($T_C$) determined using a parametrized effective Hamiltonian based on LDA[7]. However, this problem was resolved by applying a negative pressure to the system[7]. Also, the value of $T_C$ of $PbTiO_3$ using interaction parameters (calculated using LDA) at the experimental lattice constant is underestimated[8]. On the other hand, the gradient density approximation (GGA) mostly overestimates the lattice constants and gives supertetragonal structures of $PbTiO_3$ and $BaTiO_3$[14]. By including the density gradient, GGAs can predict accurate structures or energies, but not both together[15,16]. This suggests an important avenue for further functional development which can correctly capture structural properties, i.e., lattice constant, anharmonic coupling between phonon modes and strain-phonon coupling parameters, which are relevant to the structural transition. The GGA functional proposed by Wu and Cohen (WC-GGA) has been known to accurately calculate the ferroelectric properties of $BaTiO_3$ and $PbTiO_3$[17]. However, the WC-GGA fails to precisely determine the properties of atoms and molecules, as it was constructed for solids (slowly varying electron density)[17].

The recently-developed nonempirical strongly constrained and appropriately normed semilocal density functional (SCAN) has been shown to estimate accurate structures and energetics of diversely bonded molecules and materials (for slowly as well as rapidly varying electron densities) and to improve the band gap, which was underestimated by LDA and GGA[18–21]. The SCAN meta-GGA satisfies all the 17 known exact constraints (about 6 for exchange, 6 for correlation and 5 for the sum of two) appropriate to semilocal functionals by including the orbital kinetic energy densities[18]. The calculations are computationally more expensive using SCAN meta-GGA than normal GGA or LDA, but SCAN is more efficient than hybrid functionals due to its semilocal nature.

Here, we present the ground-state properties of eight perovskites, i.e., $BaTiO_3$, $CaTiO_3$, $SrTiO_3$, $PbTiO_3$, $KNbO_3$, $NaNbO_3$, $PbZrO_3$ and $BaZrO_3$ using the SCAN meta-GGA functional, and notice a significant improvement of lattice constants and band gaps of eight oxides compared to earlier theoretical results using LDA[4]. We then estimate $T_C$'s of $BaTiO_3$, $PbTiO_3$ and $KNbO_3$ using the parametrized effective Hamiltonian based on the SCAN meta-GGA functional, calculate the lowest-order coupling between soft mode and higher energy modes, and determine the consequences of approximations in construction of the effective Hamiltonian for finite-temperature properties.

## II. METHODS

First-principles calculations based on density functional theory have been performed here on eight perovskites using the SCAN meta-GGA exchange-correlation functional as implemented in the VASP code[18,22,23]. For calculations, we use plane-wave augmented (PAW) potentials containing a contribution from kinetic energy density of core electrons[24]. We have considered eight oxides, i.e., $BaTiO_3$, $SrTiO_3$, $PbTiO_3$, $CaTiO_3$, $KNbO_3$, $NaNbO_3$, $PbZrO_3$ and $BaZrO_3$, for determining ground-state properties. We use 5$s$ and 5$p$ states of Ba, 3$s$ state (3$s$ and 3$p$ states) of K (Ca), 4$s$ and 4$p$ states of Sr, Zr and Nb, 2$p$ state of Na and 5$d$ state of Pb as valence states. An energy cutoff of 560 eV has been used to truncate the plane-wave basis used to represent wave functions. Integrations over Brillouin zone were sampled on an $8 \times 8 \times 8$ uniform mesh of k-points.

MD simulations for studying the phase transitions of $BaTiO_3$, $PbTiO_3$ and $KNbO_3$ (considering the effective Hamiltonian from Ref. 7) are performed using the FERAM code[7,25,26]. At each temperature in our simulation within the canonical ensemble, temperature is kept fixed using the Nose-Poincare thermostat[27]. The time step was set to $\Delta$t=2 fs. We use a supercell of system size $L_x \times L_y \times L_z = 16 \times 16 \times 16$ and temperature step ± 5 K in heating-up and cooling-down simulations. We use 20,000 thermalization steps and 40,000 steps for averaging properties of the system at each temperature. The initial configuration used in cooling-down simulations of all three compounds is a paraelectric state with $\langle u_\alpha \rangle$=0.0 ($\alpha$=x,y,z) and $\langle u_\alpha^2 \rangle$-$\langle u_\alpha \rangle^2$=(0.12 Å$)^2$. In the heating-up simulation, we choose ferroelectric states of three compounds ($\langle u_z \rangle$=0.33 Å and $\langle u_x \rangle$=$\langle u_y \rangle$=0.0 for $PbTiO_3$ and $\langle u_\alpha \rangle$=0.11 Å for $BaTiO_3$ and $KNbO_3$) as initial configurations.

## III. RESULTS AND DISCUSSION

### A. Ground-state properties

#### 1. *structural and electronic properties*

We optimized lattice parameters of cubic perovskite structures of eight $ABO_3$ compounds, i.e., $BaTiO_3$, $SrTiO_3$, $CaTiO_3$, $PbTiO_3$, $KNbO_3$, $NaNbO_3$, $PbZrO_3$ and $BaZrO_3$, using the SCAN meta-GGA functional. Our results in comparison with LDA are shown in FIG. 1[4]. The lattice constants of cubic $SrTiO_3$, $CaTiO_3$, $PbZrO_3$ and $BaZrO_3$ are overestimated slightly by 0.1-0.5% (see FIG. 1) whereas for other compounds lattice constants are underestimated at the most by 0.8% relative to the experimental values[4]. Lattice constants optimized using SCAN are better compared to the earlier theoretical results obtained from calculations considering all-electron (FLAPW) and ultrasoft pseudopotentials with LDA[4]. Lattice parameters of cubic $BaTiO_3$, $PbTiO_3$ and $SrTiO_3$ are overestimated by 0.2% from the values obtained using the WC-GGA functional[7].

We then optimized lattice constants of the tetragonal phases of $BaTiO_3$ and $PbTiO_3$ (as shown in TABLE I). The SCAN-based calculated values of $\boldsymbol{a}$ of tetragonal phases of $BaTiO_3$ and $PbTiO_3$ are within 0.025% of experimental values and are better than earlier theoretical results using LDA, PBE-GGA and hybrid functionals[14]. The generalised gradient approximation (GGA) in the PBE parametrized form overestimates lattice constants and gives supertetragonal structures of $BaTiO_3$ and $PbTiO_3$ (see TABLE I). In addition, the differences in the z components of atomic positions between cubic and tetragonal phases of $BaTiO_3$ (ferroelectric distortion) are slightly overestimated compared to experimental values and are better than earlier theoretical results using LDA, PBE-GGA and hybrid functionals[14]. For $PbTiO_3$, the level of agreement between experiment and our estimates of these differences in atomic positions is not that good. This overestimation of atomic displacements is caused by the slight overestimation of $\boldsymbol{c}/\boldsymbol{a}$ ratios of $PbTiO_3$ (see TABLE I). We analyzed this in depth, and found that the energy surface of $PbTiO_3$ is very flat (shallow) and small energy differences result in large changes in structural parameters. However, our estimates of $\boldsymbol{c}/\boldsymbol{a}$ ratios of tetragonal $BaTiO_3$ and $PbTiO_3$ are better than those of other functionals (LDA, PBE-GGA and hybrid)[14]. Our results for $BaTiO_3$ and $PbTiO_3$ are comparable to the earlier results obtained using the WC-GGA functional and treating Ti and O atoms at the all-electron level (HF pseudopotentials for Pb and Ba)[14]. For $KNbO_3$, the $\boldsymbol{c}/\boldsymbol{a}$ ratio (1.034) is slightly overestimated with SCAN compared to the experimental value (1.017)[28]. In addition, we optimized lattice parameters of orthorhombic ($a$, $b$ and $c$) and rhombohedral ($a$ and $\alpha$) structures of $BaTiO_3$ and $KNbO_3$ using SCAN metaGGA functional (see TABLE II). Our SCAN metaGGA-based estimates of lattice parameters of orthorhombic and rhombohedral phases are within 0.4% of experimental values[29–31]. The agreement with experiment is much better than that obtained with PBE-GGA and WC-GGA functionals[32].

Elastic constants of cubic perovskites have been determined from the stress-strain relationship. The elastic constants of $BaTiO_3$ using SCAN are comparable to the value obtained using LDA (see TABLE III). The values of bulk modulus of $KNbO_3$ and $PbTiO_3$ are 197 GPa and 203 GPa respectively, which agree to about 2% with the values obtained earlier using LDA[4]. For $SrTiO_3$, elastic constants are within 16% of the experimental values[33]. It has been observed experimentally that $C_{11}$, $C_{12}$ and $C_{44}$ of $SrTiO_3$ are strong functions of temperature, and decrease by 4% when temperature drops from 30 °C to -160 °C[34]. The dependence of elastic constant on temperature has also been noticed experimentally for $BaTiO_3$ and $PbTiO_3$[35]. As first-principles based DFT calculations do not include the effect of temperature, we consider this deviation of elastic constants from the experimental values as acceptable. The exchange-correlation functional influences mostly $C_{11}$ and $C_{12}$ parameters for all materials. SCAN-based estimates of $C_{11}$ are overestimated compared to experimental values whereas other elastic constants are close to experimental values (see TABLE III)[33,36].

Our calculated direct band gaps at the X point (of $PbTiO_3$ and $PbZrO_3$) and at the $\Gamma$ point (of other compounds) of cubic perovskites (at optimized lattice constant) in comparison with earlier theoretical and experimental results are presented in FIG. 2[4,33,37–41]. SCAN gives a better estimation of band gaps of perovskites and other materials[20,21] compared to LDA[4,18,19]. LDA underestimates the band gaps by 40-50%. The band gaps in SCAN are also underestimated, but are modestly improved over LDA.

Next, we determine the effect of the exchange-correlation functional on vibrational properties which have important consequences for the finite-temperature properties of perovskites.

### 2. *Vibrational properties*

For the five-atom unit cell of cubic phase of perovskites, there are twelve optical phonon modes at $\Gamma$ point. Out of twelve optical modes, three triply-degenerate phonon modes have $\Gamma_{15}$ symmetry and one triply-degenerate mode has $\Gamma_{25}$ symmetry. The eigenvector of the phonon mode with $\Gamma_{25}$ symmetry involves atomic displacements along the z direction as ($v_z^A$=0, $v_z^B$=0, $v_z^{O_I}=\frac{1}{\sqrt{2}}$, $v_z^{O_{II}}$=-$\frac{1}{\sqrt{2}}$ and $v_z^{O_{III}}$=0). Phonon modes with $\Gamma_{15}$ symmetry are relevant to the ferroelectric transition[4]. One of the eigenvalues of the phonon modes with $\Gamma_{15}$ symmetry of the cubic phase becomes negative (for the five-atom unit cell as experimental ground state), which indicates the cubic phase to be unstable. We have compared the optical phonon frequencies (see TABLE IV) obtained at the optimized lattice constant with earlier theoretical calculations based on LDA, GGA and hybrid functionals and experimentally-measured frequencies[14,42,43]. Our estimated zone-centre optical phonon frequencies (TO1, TO2, TO3 and TO4) of $BaTiO_3$ and $SrTiO_3$ using SCAN are in excellent agreement (within 3% for $BaTiO_3$ and 8% for $SrTiO_3$) with experimental values and are better compared to earlier estimates calculated using LDA, GGA and hybrid functionals[14]. For $PbTiO_3$, our calculated phonon frequencies differ by 19% from earlier theoretical results (using LDA, GGA and hybrid functionals)[14]. Phonon frequencies of cubic $PbTiO_3$ can not be readily compared with experimental values, as the literature is not available. SCAN predicts phonon frequencies much closer to the experimental values for cubic $KNbO_3$ compared to earlier LDA calculations[42]. Moreover, our predicted phonon frequencies (of $BaTiO_3$, $SrTiO_3$ and $KNbO_3$) are better than earlier theoretically-calculated values using different functionals[14,42,43].

We now examine the eigenvalues of unstable phonon modes (TO1) with $\Gamma_{15}$ symmetry (see TABLE V). We find that the value of the harmonic coupling parameter $\kappa$ is positive (see TABLE V) for cubic $BaZrO_3$, which assumes the cubic phase at all temperature, and is consistent with the earlier LDA result and experimental findings[4]. The positive value of $\kappa$ for $SrTiO_3$ is consistent with the antiferrodistortive transition associated with phonon mode at $q \neq 0$. In contrast, earlier LDA results gave a negative value of $\kappa$ for $SrTiO_3$[4], while another LDA calculation with high plane-wave kinetic energy cutoff (50 Ry) predicts a positive value (0.096 eV/$\text{Å}^2$) of $\kappa$ of $SrTiO_3$. For other compounds, the value of $\kappa$ is found to be negative which is in agreement with earlier theoretical results using LDA (see TABLE V). Overall, our calculated values of $\kappa$'s are more negative for $BaTiO_3$, $KNbO_3$ and $NaNbO_3$ compared to earlier LDA results whereas they are more positive for other compounds, which are relevant for defining the potential energy surface[4].

The eigenvector of the soft mode of the cubic structure and its amplitude in the ferroelectric phase of $BaTiO_3$ (see TABLE VI) are comparable to the eigenvector obtained earlier using LDA[4] although the lattice constants obtained using the two functionals are quite different. On the other hand, the displacement of the Pb atom associated with the soft mode is large compared to the value obtained using LDA, although amplitudes of soft modes using the two different functionals are similar[4]. Eigenvectors of the soft modes of $NaNbO_3$ and $CaTiO_3$ obtained using the two functionals (SCAN and LDA) are slightly different from each other[4]. For other compounds, eigenvectors and amplitudes of the soft modes are comparable with the results estimated earlier using LDA[4]. Our calculated eigenvector of the soft mode of $BaTiO_3$ is similar to the eigenvector obtained using the WC-GGA functional[7].

Anharmonic coupling coefficients $\alpha$ and $\gamma$ in the on-site energy are determined from the expressions for energy as a function of soft mode amplitude (u) along [001] and [111] directions (up to fourth-order terms in u)[4]:

$$E_{001}(u) = \kappa u^2 + \alpha u^4, \tag{1a}$$

$$E_{111}(u) = 3\kappa u^2 + (9\alpha + 3\gamma)u^4. \tag{1b}$$

The energies of unstrained cubic $PbTiO_3$ and $BaTiO_3$ as a function of soft mode displacements are shown in FIG. 3. When strain is not applied, the rhombohedral phase has minimum energy for $BaTiO_3$ and $PbTiO_3$ (as shown in FIG. 3), consistent with earlier LDA results[4]. The depth of the double-well (as shown in FIG. 3) is larger for $PbTiO_3$ compared to $BaTiO_3$ as the values of $\alpha$ and $\gamma$ (obtained using SCAN) of $PbTiO_3$ are small (see TABLE V).

We compute strain-phonon coupling parameters to find the ground state of each oxide. Strain-phonon coupling parameters ($B_{1xx}$, $B_{1yy}$ and $B_{4yz}$) of the eight perovskites are determined by calculating the change in the values of $\kappa$ with strain. Changes in the eigenvalues of an x-polarized soft mode ($\kappa_x$) with the applications of strains along x ($\eta_1$) and y directions ($\eta_2$) give $B_{1xx}$ and $B_{1yy}$ respectively (as shown in see FIG. 4). To find the value of $B_{4yz}$, we calculate the change in the value of $\kappa$ of the soft mode distortion along [111] direction with the change of shear strain ($\eta_4$). We notice that strain-phonon coupling parameters are sensitive to the exchange-correlation functional (see TABLE V). $B_{1yy}$ and $B_{4yz}$ coupling parameters of $BaTiO_3$ and $PbTiO_3$ mostly get affected by the exchange-correlation functional. For $NaNbO_3$, $PbZrO_3$ and $BaZrO_3$, $B_{1xx}$ even changes its sign with the change of exchange-correlation functional. We consider these calculated parameters to obtain the ground state of every compound, as discussed below.

Using the fourth-order expansion of energy as a function of soft mode amplitude and strain, the energy differences between cubic ($E_C$), tetragonal ($E_T$), orthorhombic ($E_O$) and rhombohedral ($E_R$) phases are[4]:

$$E_C - E_T = -\frac{\kappa^2}{4\alpha'}, \tag{2a}$$

$$E_C - E_O = -\frac{\kappa^2}{4\alpha' + \gamma'}, \tag{2b}$$

$$E_C - E_R = -\frac{\kappa^2}{4(\alpha' + \gamma'/3)}. \tag{2c}$$

$\alpha'$ and $\gamma'$ are renormalized anharmonic coupling constants (as given in equations 11b, 12b and 13b in Ref. 4) which depend on elastic constants, strain-phonon coupling parameters and bare anharmonic coupling constants ($\alpha$ and $\gamma$).

We find that the value of $\gamma$ is typically negative as shown in TABLE V. The introduction of strain switches the sign of $\gamma$ in some cases, which highlights the importance of strain-phonon coupling. If $\kappa$ is less than zero, stability of tetragonal and rhombohedral ground states require $\gamma'$ to be greater and less than zero respectively (using equations 2a-2c). Negative values of $\gamma'$ of $BaTiO_3$, $KNbO_3$, $NaNbO_3$ and $PbZrO_3$ mean that the ground state is rhombohedral, which is consistent with earlier theoretical results using LDA[4]. For $PbTiO_3$ and $CaTiO_3$, the tetragonal state is the ground state as $\gamma'$ is positive (consistent with earlier LDA results[4]). In addition, cubic phases of $SrTiO_3$ and $BaZrO_3$ have minimum energy as $\kappa$ is positive. The experimentally-observed ground states for $SrTiO_3$, $CaTiO_3$ and $NaNbO_3$ are tetragonal (antiferrodistortive transition associated with oxygen octahedra rotation), orthorhombic (with 20 atoms in the unit cell) and monoclinic phase (20 atoms per unit cell) respectively[4]. Hence, these can not be explained using the fourth-order expansion of energy, which considers only the soft mode at the Γ point.

The calculated energy difference between cubic and tetragonal phases (using equation 2a) of $BaTiO_3$, $PbTiO_3$ and $KNbO_3$ are 16 meV/unit cell (12 meV/unit cell, LDA), 95 meV/unit cell (58 meV/unit cell, LDA) and 43 meV/unit cell (8 meV/unit cell, LDA) respectively (as shown in FIG. 5). For $BaZrO_3$, the energy difference between cubic and tetragonal phase is 1.3 eV/unit cell which is much larger compared to the value (45 meV/unit cell) obtained using the parameters from earlier theoretical calculations using LDA[4]. For comparison of energy difference between cubic and tetragonal phases of $CaTiO_3$, we use parameters from another calculations (with LDA) with a high plane-wave kinetic energy cutoff (50 Ry)[44]. SCAN produces deeper potential wells (energy as a function of soft mode amplitude and strain) for all compounds, in comparison with earlier theoretical results using LDA[4,44]. Depths of the potential well along the [110] and [111] directions (using equations 2b and 2c) are (19 meV/unit cell, 20 meV/unit cell) for $BaTiO_3$ and (46 meV/unit cell, 47 meV/unit cell) for $KNbO_3$ respectively. Our calculated energy differences (orthorhombic and rhombohedral) are larger compared to the depth obtained using LDA-based parameters ($BaTiO_3$: 14 meV/unit cell and 15 meV/unit cell, $KNbO_3$: 9 meV/unit cell and 10 meV/unit cell). As the depths of double-well energy surfaces are believed to be underestimated in the LDA framework, the description of total energy surfaces gets improved by the accurate estimation of lattice constants using SCAN.

## B. Finite temperature properties

We now investigate the effect of the exchange-correlation functional on finite-temperature properties, i.e., transition temperatures of three compounds ($BaTiO_3$, $PbTiO_3$ and $KNbO_3$) whose ferroelectric transitions are associated with the soft mode at the $\Gamma$ point.

### 1. *Effective Hamiltonian*

To predict the finite-temperature properties using MD simulation, we use an effective Hamiltonian[7,25]:

$$\begin{aligned} H^{eff} = \frac{M^*_{dipole}}{2} \sum_{\boldsymbol{R},\alpha} \dot{u}^2_\alpha(\boldsymbol{R}) + V^{self}(\{\boldsymbol{u}\}) + V^{dpl}(\{\boldsymbol{u}\}) + \\ V^{short}(\{\boldsymbol{u}\}) + V^{elas,homo}(\eta_1, ..., \eta_6) + V^{coup,homo}(\{\boldsymbol{u}\}, \eta_1, ..., \eta_6) \end{aligned} \tag{3}$$

where **u** and **w** are the local soft mode amplitude vector (soft mode displacement vector) and acoustic mode displacement vector (lattice Wannier mode[45]) of the unit cell at position R respectively ($\alpha$=x,y,z). $\eta_1$, ..., $\eta_6$ are the homogeneous strain components. $M^*_{dipole}$ and $M^*_{acoustic}$ are effective masses associated with polar soft and acoustic modes respectively. $Z^*$ is the Born effective charge associated with the soft mode, and $\mathcal{E}$ is the external electric field.

The third term in equation 3 represents local-mode self energy ($V^{self}(\mathbf{u})$)[7]:

$$\begin{aligned} V^{self}(\{\boldsymbol{u}\}) = \sum_{\boldsymbol{R}} & \kappa_2 u^2(\boldsymbol{R}) + \alpha u^4(\boldsymbol{R}) + \gamma(u_x^2(\boldsymbol{R})u_y^2(\boldsymbol{R}) + u_y^2(\boldsymbol{R})u_z^2(\boldsymbol{R}) + u_z^2(\boldsymbol{R})u_x^2(\boldsymbol{R})) \\ & + k_1 u^6(\boldsymbol{R}) + k_2(u_x^4(\boldsymbol{R})[u_y^2(\boldsymbol{R}) + u_z^2(\boldsymbol{R})] + u_y^4(\boldsymbol{R})[u_z^2(\boldsymbol{R}) + u_x^2(\boldsymbol{R})] \\ & + u_z^4(\boldsymbol{R})[u_x^2(\boldsymbol{R}) + u_y^2(\boldsymbol{R})]) + k_3 u_x^2(\boldsymbol{R})u_y^2(\boldsymbol{R})u_z^2(\boldsymbol{R}) + k_4 u^8(\boldsymbol{R}), \end{aligned} \tag{4}$$

where $u^2(\mathbf{R}) = u_x^2(\mathbf{R}) + u_y^2(\mathbf{R}) + u_z^2(\mathbf{R})$.

Equations 1a and 1b can be obtained from equation 4 by taking $\mathbf{u}(\mathbf{R})$=(0,0,u) and $\mathbf{u}(\mathbf{R})$=(u,u,u) and replacing $\kappa_2$ to $\kappa$ and truncating the polynomial in u at the fourth-order terms. The fourth and fifth terms in equation 3 represent long-range dipole-dipole interaction and short-range harmonic interaction between optical displacements ($\mathbf{u}(\mathbf{R})$) up to third nearest neighbors. Terms containing acoustic mode displacement vector ($\mathbf{w}(\mathbf{R})$) have been integrated out by minimizing equation 3 with respect to ($\mathbf{w}(\mathbf{R})$)[25]. Sixth and eighth terms in equation 3 are the elastic energy and coupling between homogeneous strain and optical mode ($\mathbf{u}$), which have been determined here by using the coupling constants (elastic constant ($C_{\alpha\beta\gamma\delta}$) and strain-phonon coupling ($B_{i\alpha\beta}$) parameters) as discussed in the earlier section. We did not include the effect of external electric field.

The short-range and long-range interaction parameters determine the energy (or frequency) of the soft mode at high symmetry points other than Γ. We determine phonon spectra at X, M and R points of the Brillouin zone of $BaTiO_3$, $PbTiO_3$ and $KNbO_3$ to calculate the short-range interaction parameters. These phonon calculations (at X, M and R points) were performed with (1×1×2), ($\sqrt{2}\times\sqrt{2}\times1$) and ($\sqrt{2}\times\sqrt{2}\times\sqrt{2}$) supercells containing 10 atoms each respectively. In addition, we calculate phonon modes at the centre of the Σ axis (q=(110)$\frac{\pi}{2a}$) by considering $2\sqrt{2}\times1\times\sqrt{2}$ supercell with 20 atoms for $PbTiO_3$. We should note that these calculations use the cubic structure of these compounds. The long-range dipole-dipole interaction is proportional to $Z^{*2}/\epsilon_\infty$, where $Z^*$ is the mode effective charges associated with the soft mode and $\epsilon_\infty$ is the dielectric constant[10]. Our calculated values of $Z^*$ are 10.16 ($BaTiO_3$), 9.37 ($PbTiO_3$) and 11.52 ($KNbO_3$), $M^*$ are 37.5 amu ($BaTiO_3$), 102.6 amu ($PbTiO_3$), 65.4 amu ($KNbO_3$) and $\epsilon_\infty$ are 6.27 ($BaTiO_3$), 7.95 ($PbTiO_3$) and 5.492 ($KNbO_3$). While the SCAN meta-GGA estimates of $Z^{*2}/\epsilon_\infty$ are within 10% of the LDA estimates, they are closer (within 5%) to the Wu-Cohen functional based estimates available for $KNbO_3$ and $BaTiO_3$[7,32]. We consider local modes with Ti and Nb centered atomic displacements (at Γ, X, M and R points) to study the phase transitions in $BaTiO_3$ and $KNbO_3$[45]. However, Pb centered local modes (at Γ, X, M and R points) have been used here to study the phase transition in $PbTiO_3$[8]. For studying phase transitions, we use the eigenvalues of doubly-degenerate modes with $X_5$ ($X_5{}'$ mode for $PbTiO_3$) and $M_5{}'$ ($M_5{}'$

mode for $PbTiO_3$) symmetries, nondegenerate modes with $X_1$ ($X_2'$ mode for $PbTiO_3$) and $M_3'$ ($M_2'$ mode for $PbTiO_3$) symmetries and triply-degenerate mode with $R_{25}'$ ($R_{15}$ mode for $PbTiO_3$) symmetry of $KNbO_3$ and $BaTiO_3$. We also take into account one Pb-based optical phonon mode at $(110)\frac{\pi}{2a}$ point of $PbTiO_3$. The local ($\kappa_2$) and short-range interaction parameters ($j_1$,...,$j_7$) are determined by using the eigenvalues ($\omega$'s) of these selected phonon modes and solving the linear equations as given in Refs. 7,8 and 10.

The total harmonic interaction (long- and short-range) matrix $\tilde{\Phi}^{quad}(\mathrm{k})$ is analyzed using FERAM[7,26] to get the model phonon dispersion of $BaTiO_3$ (see FIG. 6), which is similar to the dispersion obtained in earlier simulations using WC-GGA-based parameters[7]. The short-range interaction gives the most unstable mode at the X point (see FIG. 6a). The dipole-dipole long-range interaction term results in a cell-doubling state due to the strongest instability at the M point[25]. The long-range dipole-dipole interaction splits the longitudinal and transverse optical phonon modes at the $\Gamma$ point (see FIG. 6b) and the splitting in $\omega$ is proportional to $Z^{*2}/\epsilon_\infty$. However, the competing short and long-range interactions together give the strongest instability at the $\Gamma$ point. The short-range interaction parameters of $BaTiO_3$, $PbTiO_3$ and $KNbO_3$ are given in TABLE VII. For $BaTiO_3$, the short-range interaction parameters are comparable to the parameters based on earlier calculations using WC-GGA. As LDA underestimates lattice constants, the local ($\kappa_2$) and short-range interaction parameters ($j_2$, $j_5$ and $j_7$) calculated earlier using LDA are different from our estimates. The short-range interaction parameters of $PbTiO_3$ obtained using SCAN are similar to the values obtained using LDA at the experimental lattice constant (partly justifying this approximation in Ref. 8)[8,46]. For $KNbO_3$, local ($\kappa_2$) and short-range interaction parameters ($j_1$, $j_2$ and $j_4$) are different from earlier theoretical results using WC-GGA[26].

### 2. *MD simulations*

Using a SCAN-based parametrized effective Hamiltonian (truncating the local-mode self energy up to fourth-order terms in u in equation 4)[10,25], we perform heating-up and cooling-down molecular dynamics simulations for $BaTiO_3$, $PbTiO_3$ and $KNbO_3$ to estimate $T_C$'s. We define $T_C$ for the phase transition P↔Q to be the mean of the transition temperatures for P→Q and Q→P. Simulated lattice parameters of these compounds as a function of temperature are presented in FIG. 7. For $BaTiO_3$ and $KNbO_3$, we find three transitions: from cubic (C) to tetragonal (T), from tetragonal (T) to orthorhombic (O) and from orthorhombic (O) to rhombohedral (R), which are consistent with the experimental observations[42,47]. We find a single structural transition from cubic to tetragonal phase in $PbTiO_3$.

Our predicted transition temperatures of $BaTiO_3$ (see TABLE VIII) are $T_C$ (C↔T) = 213 K, $T_C$ (T↔O)=141 K and $T_C$ (O↔R)=111 K (see FIG. 7a). $T_C$'s of $BaTiO_3$ are underestimated by up to 65% with respect to the experimental transition temperatures[47]. However, our $T_C$'s are 45% higher than earlier results obtained using LDA at zero pressure[7]. The accurate determination of total energy surfaces using SCAN gets reflected in the estimates of the transition temperatures. The rhombohedral to orthorhombic transition temperature is improved compared to earlier LDA and WC-GGA results at zero pressure[7]. The $T_C$'s of the transitions from orthorhombic phase to tetragonal phase and tetragonal to cubic phase are 29% lower than the $T_C$'s obtained with parameters obtained using the WC-GGA functional at zero pressure[7]. The $\boldsymbol{c/a}$ ratio of the tetragonal phase obtained using the SCAN-based parametrized effective Hamiltonian is 1.009 at 150 K which agrees very well with the experimental value (1.01)[14]. Earlier MD simulations using the WC-GGA-based parameters gave $\boldsymbol{c/a}$ ratio of the tetragonal phase (1.017 at 155 K) higher than the experimental value[7,14]. It has been observed from earlier results that the tetragonal to cubic transition temperature changes drastically by the application of negative pressure, whereas the two other $T_C$'s do not depend strongly on pressure. As our calculated strain-phonon coupling parameters are distinct from these in earlier works ($B_{1xx}$=-185.33 eV/Å$^2$ and $B_{1yy}$=-3.28 eV/Å$^2$) using the WC-GGA functional, the transition temperatures estimated with these two functionals are different[7].

Our estimated three transition temperatures (see TABLE VIII) of $KNbO_3$ (O↔R=160 K, T↔O=225 K and C↔T=540 K) using the SCAN-based parameters (see FIG. 7b) are underestimated compared to the experimental $T_C$'s (O↔R=210 K, T↔O=488 K and C↔T=701 K) with largest error for T↔O transition[42]. Values of $T_C$ (T↔O) and $T_C$ (O↔R) calculated here are slightly underestimated compared to earlier LDA results at the experimental lattice constant[48]. However, our calculated $T_C$ (C↔T) is much larger compared to earlier LDA results at the experimental lattice constant[48]. On the other hand, our predicted transition temperatures are lower than the calculated $T_C$'s using the WC-GGA functional at zero pressure[26]. The optimized lattice parameter of cubic $KNbO_3$ using SCAN is similar to the earlier computed value using the WC-GGA functional[26]. However, the inclusion of higher-order (greater than 4) on-site anharmonic coupling parameters, drastically different strain-phonon coupling parameters ($B_{1xx}$=-220.45 eV/Å$^2$ and $B_{1yy}$=31.35 eV/Å$^2$) in earlier WC-GGA calculations result in different values of $T_C$'s compared to our estimated values[26]. We must note that application of negative pressure (using WC-GGA based effective Hamiltonian for $BaTiO_3$ and $KNbO_3$) does not affect the two lowest structural transition temperatures (O↔R and T↔O), whereas only $T_C$ (C↔T) is a strong function of pressure[7,26]. The WC-GGA functional has been constructed with a particular focus on ferroelectric materials[7,17]. On the other hand, the SCAN meta-GGA functional is universal as it is applicable for all diversely bonded materials but might fail to determine precisely one specific property of a particular type of material. However, SCAN removes the typical error in estimating $T_C$'s arising from the underestimation of lattice constant.

For $PbTiO_3$, we find a cubic to tetragonal phase transition at 630 K (see FIG. 7c), which is slightly lower than the experimental $T_C$ = 763 K (see TABLE VIII). However, our predicted $T_C$ is close to earlier calculated $T_C$ (635 K) based on LDA parameters at the experimental lattice constant[49]. The tetragonal $\boldsymbol{c}/\boldsymbol{a}$ ratio at 0 K (obtained by extrapolating lattice parameters) is 1.104 which is overestimated compared to the experimental value (1.071 at 0 K)[14]. It is clear that SCAN-based predictions of the transition temperatures of the three oxides improve over those of LDA-based parameters[8,46].

The discrepancies between our calculated $T_C$'s and experimental $T_C$'s have a contribution from the neglect of the anharmonic coupling between the soft mode and higher energy phonon modes, as the error in lattice constant has been minimized using the SCAN meta-GGA functional. The effect of including anharmonic coupling between soft and higher-energy modes on finite temperature properties will be discussed in the following section.

### C. Anharmonic coupling between phonons

We find that the depths of the double-well potentials of $BaTiO_3$, $PbTiO_3$ and $KNbO_3$ (along the [001] direction) obtained directly from DFT calculations ($E_{cubic}$-$E_{tetragonal}$=25 meV/unit cell for $BaTiO_3$, 123 meV/unit cell for $PbTiO_3$ and 47 meV for $KNbO_3$) and from the effective Hamiltonian (equation 2a) written as a fourth-order expansion (16 meV/unit cell for $BaTiO_3$, 95 meV/unit cell for $PbTiO_3$ and 43 meV for $KNbO_3$) are different. This difference in energies highlights the presence of anharmonic coupling between the soft mode and other higher-energy optical phonon modes.

To identify higher-energy optical modes responsible for the phase transition, we define a vector given as:

$$\vec{S} = \vec{f} - (\vec{f}.\hat{e}_{soft})\hat{e}_{soft}, \tag{5}$$

where $\hat{e}_{soft}$ is the soft mode eigenvector and $\vec{f}$ is the ferroelectric distortion given as atomic displacement vector from the cubic to tetragonal phase. Phonon modes having $\Gamma_{15}$ symmetry with frequencies 182 cm$^{-1}$ (for $BaTiO_3$), 140 cm$^{-1}$ (for $PbTiO_3$) and 207 cm$^{-1}$ (for $KNbO_3$) show strong overlap (0.79 for $BaTiO_3$, 0.55 for $PbTiO_3$ and 0.52 for $KNbO_3$) with $\hat{S}$. We find higher-energy optical phonon modes with $\Gamma_{15}$ symmetry (478 cm$^{-1}$ for $BaTiO_3$, 530 cm$^{-1}$ for $PbTiO_3$ and 483 cm$^{-1}$ for $KNbO_3$) contributing sizably to the ferroelectric distortion of the cubic phase.

To model the lowest-order coupling between these $\Gamma_{15}$ modes, we write the total energy (along the [001] direction) as a function of soft mode (u), higher-energy modes $v_1$ (182 cm$^{-1}$

for $BaTiO_3$, 140 cm$^{-1}$ for $PbTiO_3$ and 207 cm$^{-1}$ for $KNbO_3$) and $v_2$ (478 cm$^{-1}$ for $BaTiO_3$, 530 cm$^{-1}$ for $PbTiO_3$ and 483 cm$^{-1}$ for $KNbO_3$) by expanding it as a symmetry-invariant Taylor series expansion up to eighth-order in u and second-order in $v_1$ and $v_2$ with respect to the cubic phase using ISOTROPY[50]:

$$E(u, v_1, v_2) = \kappa u^2 + \alpha' u^4 + k_1 u^6 + k_4 u^8 + \kappa_{v_1} v_1^2 + e_1 u^3 v_1 + f_1 u^2 v_1^2 + \kappa_{v_2} v_2^2 + e_2 u^3 v_2 + f_2 u^2 v_2^2 \quad (6)$$

We have not considered the cubic coupling terms in higher energy phonon modes as their contributions to the energy are less significant. $e_1$ and $e_2$ have been determined by projecting forces (arising due to the freezing of the soft mode) on $v_1$ and $v_2$ as shown in FIG. 8a and FIG. 8b respectively. $f_1$ and $f_2$ coupling terms have been evaluated by calculating the eigenvalues of $v_1$ and $v_2$ modes as a function of amplitude of the soft mode (u), shown in FIG. 8c and FIG. 8d respectively. Such anharmonic coupling between the soft mode and higher-energy optical phonon modes was ignored in the earlier model Hamiltonian (equation 4).

Minimizing the total energy (equation 6) with respect to $v_1$ and $v_2$, the resulting $v_{1,min}$ and $v_{2,min}$ are:

$$v_{1,min} \approx -\frac{e_1 u^3}{2k_{v_1}}(1 - \frac{f_1}{\kappa_{v_1}} u^2), \quad (7a)$$

$$v_{2,min} \approx -\frac{e_2 u^3}{2k_{v_2}}(1 - \frac{f_2}{\kappa_{v_2}} u^2). \quad (7b)$$

The renormalized form of the total energy as a function of u is obtained by substituting $v_{1,min}$ and $v_{2,min}$ in equation 6:

$$\begin{aligned} E(u) &= \kappa u^2 + \alpha' u^4 + (k_1 - \frac{e_1^2}{4\kappa_{v_1}} - \frac{e_2^2}{4\kappa_{v_2}})u^6 + (k_4 - \frac{e_1^2 f_1}{4\kappa_{v_1}^2} - \frac{e_2^2 f_2}{4\kappa_{v_2}^2})u^8, \\ &= \kappa u^2 + \alpha' u^4 + k_1' u^6 + k_4' u^8. \end{aligned} \quad (8)$$

The fourth-order coupling terms between phonon modes modify the terms associated with sixth- and eighth-order in soft-mode displacement.

The expressions for total energies as a function of u along [110] and [111] directions are[7]:

$$E_{110}(u) = \kappa u^2 + (\alpha' + \frac{1}{4}\gamma')u^4 + (k_1' + \frac{1}{4}k_2)u^6 + k_4' u^8, \quad (9a)$$

$$E_{111}(u) = \kappa u^2 + (\alpha' + \frac{1}{3}\gamma')u^4 + (k_1' + \frac{2}{9}k_2 + \frac{1}{27}k_3)u^6 + k_4' u^8. \quad (9b)$$

For $BaTiO_3$, the values of the coupling constants are 3.95 eV/Å$^2$ ($k_{v_1}$), 6.85 eV/Å$^2$ ($k_{v_2}$), 107.91 eV/Å$^4$ ($e_1$), 107.22 eV/Å$^4$ ($e_2$), -92.74 eV/Å$^4$ ($f_1$), 52.75 eV/Å$^4$ ($f_2$), -325.24 eV/Å$^6$

($k_1$) and 2196.59 eV/$\mathring{A}^8$ ($k_4$). We have also determined the sixth-order terms $k_2$ (407.79 eV/$\mathring{A}^6$) and $k_3$ (1286.21 eV/$\mathring{A}^6$) to define the potential energy surface for distortions along [110] and [111] directions (using equations 9a and 9b). When the double-well energy functions (along [111] and [001] directions) are fitted with an eighth-order polynomial, the values of $\alpha$ and $\gamma$ change to 126.18 eV/$\mathring{A}^4$ and -171.69 eV/$\mathring{A}^4$ respectively. However, the addition of sixth- and eighth-order terms (without including coupling between soft polar and higher energy modes) does not affect the well depth and transition temperatures. The calculated energy difference between cubic and tetragonal phases using equation 8 is 24 meV, which is closer to the value obtained from DFT calculations (25 meV).

To investigate the effect of changing the depth of double-well potential energy on finite temperature properties, we calculate the transition temperatures of $BaTiO_3$ considering our generalised effective Hamiltonian (equations 8, 9a and 9b). Our simulated three transition parameters (see TABLE VIII) using the new parameters ($k_1'$ and $k_4'$) are 230 K (O↔R), 278 K (R↔T) and 375 K (T↔C) as shown in FIG. 9a. The tetragonal to cubic transition temperature increases by 57% from the value (217 K) obtained without including the coupling between soft mode and higher energy modes. The simulated value of $\boldsymbol{c}/\boldsymbol{a}$ ratio at 300 K of the tetragonal phase is 1.014 which is slightly overestimated compared to the experimental value (1.010), as expected[14]. Here, we did not include the anharmonic coupling between phonons to modify $k_2$ and $k_3$ parameters, which will precisely determine the depth of the energy well along [111] and [110] directions. This leads to the slight overestimation of two lower $T_C$'s.

Similarly, the depth of the potential well of the tetragonal state in the model of $KNbO_3$ increases by 9 meV (from the value of 43 meV obtained using equation 2a) after including the effects of anharmonic coupling between soft-mode and higher-energy phonons ($k_{v_1}$=3.27 eV/$\mathring{A}^2$, $k_{v_2}$=7.17 eV/$\mathring{A}^2$, $e_1$=0.2 eV/$\mathring{A}^4$, $e_2$=-139.2 eV/$\mathring{A}^4$, $f_1$=-135.5 eV/$\mathring{A}^4$, $f_2$=-138.3 eV/$\mathring{A}^4$, $k_1$=-464.3 eV/$\mathring{A}^6$ and $k_4$=1658 eV/$\mathring{A}^8$, $k_2$=550 eV/$\mathring{A}^6$, $k_3$=1347 eV/$\mathring{A}^6$). It is slightly overestimated compared to the energy well depth calculated using DFT calculations (47 meV). The values of $\alpha$ and $\gamma$ changes to 127 eV/$\mathring{A}^4$ and -166 eV/$\mathring{A}^4$ (which does not affect $T_C$'s when anharmonic coupling between phonons is not included), when the double-well energy functions are fitted with an eighth-order polynomial. The calculated values of $T_C$'s of $KNbO_3$ using our generalised model Hamiltonian with SCAN-based parameters are $T_C$ (C↔T) = 565 K, $T_C$ (T↔O)=230 K and $T_C$ (O↔R)=160 K (see TABLE VIII and FIG. 9b). We notice an increase in the tetragonal to cubic transition temperature by 25 K from the value (540 K) calculated earlier here, while the other two $T_C$'s almost remain unaltered.

Furthermore, we have calculated anharmonic coupling parameters between soft mode and other two optical phonon modes ($\omega_{v_1}$=140 cm$^{-1}$ and $\omega_{v_2}$=530 cm$^{-1}$) with $\Gamma_{15}$ symmetry

($\kappa_{v_1}$=2.70 eV/Å$^2$, $\kappa_{v_2}$=7.91 eV/Å$^2$, $e_1$=41.02 eV/Å$^4$, $e_2$=28.61 eV/Å$^4$, $f_1$=-12.75 eV/Å$^4$, $f_2$=-18.27 eV/Å$^4$, $k_1$=-1.97 eV/Å$^6$ and $k_4$=13.64 eV/Å$^8$) of $PbTiO_3$. The value of $\alpha$ changes slightly (6.52 eV/Å$^4$), when the potential energy surface along [001] direction is fitted with an eighth-order polynomial and it does not affect the well depth and transition temperature. The evaluated energy difference between cubic and tetragonal phases using equation 8 is 151 meV, which is slightly overestimated compared to the value (123 meV) obtained using DFT calculation. After including anharmonic couplings between soft and higher-energy modes, We find an increase in $T_C$ to 675 K (see FIG. 9c) from the value (630 K) calculated earlier here (see TABLE VIII). The $\boldsymbol{c/a}$ ratio at 0 K (obtained by extrapolating lattice parameters) is 1.053, which is in close agreement with the experimental value (1.071 at 0 K), but some errors are expected from approximately integrating out the higher-energy optic phonons[14]. Overall, our model based on the parameters calculated using SCAN precisely determines the depth of the potential well along the [001] direction, and gives a better estimation of $T_C$'s and $\boldsymbol{c/a}$ ratios of the tetragonal phases of $BaTiO_3$ and $PbTiO_3$.

## IV. SUMMARY

We demonstrated consistent improvement in theoretical prediction of structural parameters of the eight cubic perovskite oxides using the SCAN meta-GGA functional relative to LDA or GGA. In addition, estimates of band gaps of perovskite oxides typically increase and modestly improve over the earlier estimates of band gaps obtained with LDA. Accurate structural parameters given by the SCAN meta-GGA functional allow estimation of more realistic total energy surfaces of cubic perovskites as a function of soft-mode amplitude, which are relevant to the temperature-dependent structural phase transition. Our predicted zone centre optical phonon (stable modes) frequencies using the SCAN meta-GGA functional are in better agreement with the experimentally observed frequencies compared to the values using other functionals. Elastic constants and eigenvectors of soft modes are weakly dependent on the choice of exchange-correlation energy functional. For $BaTiO_3$, $PbTiO_3$ and $KNbO_3$, the strain phonon coupling parameter $B_{4yz}$ and anharmonic coupling terms and eigenvalues of soft modes get significantly altered by the SCAN meta-GGA exchange-correlation functional. The depths of the double-well energy surfaces of the polar distortions along [001], [110] and [111] directions determined using the SCAN meta-GGA functional are notably enhanced relative to the depth obtained earlier using LDA.

As a consequence of these improvements, estimates of $T_C$'s of all the structural transitions in $BaTiO_3$ and $PbTiO_3$ are closer to experiment than those of the earlier LDA results. In particular, analysis of temperature-dependent transitions can be carried out with the

SCAN meta-GGA based energy surface without having to use negative pressure to compensate for error in lattice constants (e.g., in LDA). We have quantified the consequences of truncation of the subspace of the effective Hamiltonian using the lowest-order coupling between soft and higher energy optic modes with $\Gamma_{15}$ symmetry to estimation of $T_C$'s. The fourth-order anharmonic coupling between the soft polar mode and higher-energy optical modes in $BaTiO_3$ and $PbTiO_3$ causes the increase in the depth of the potential well, and consequently enhances the estimated $T_C$'s (Figs. 7, 9 and TABLE VIII). At the interfaces in hetero-structures or superlattices based on perovskite oxides, details of atomic-scale structure depend on the mismatch between lattice constants, and electronic band offsets depend on band-gaps. Since estimates of both lattice constants and band-gap are consistently improved with SCAN meta-GGA calculations, we expect SCAN meta-GGA to be very effective in simulations of perovskite hetero-structures.

## V. ACKNOWLEDGMENTS

A.P. is thankful for the research fellowship from the Department of Science and Technology, India and TUE - CMS, JNCASR, India for computational resources. UVW thanks support from a J C Bose National Fellowship of the Department of Science and Technology, Government of India. Our work is partly supported by the Centre for the Computational Design of Functional Layered Materials, an Energy Frontier Research Centre funded by the U.S. Department of Energy, Office of Science, Basic Energy Sciences, under Award No. DE-SC0012575.

---

* waghmare@jncasr.ac.in

[1] M. Lines and A. Glass, *Principles and Applications of Ferroelectrics and Related Materials*, International series of monographs on physics (OUP Oxford, 1977).

[2] R. Waser, *Nanoelectronics and Information Technology* (Wiley, 2012).

[3] R. E. Cohen, Nature **358** (1992).

[4] R. D. King-Smith and D. Vanderbilt, Phys. Rev. B **49**, 5828 (1994).

[5] B. Wul and J. M. Goldman, C. R. Acad. Sci. URRS **46**, 139 (1945).

[6] K. M. Rabe, *Antiferroelectricity in Oxides: A Reexamination* (Wiley-VCH Verlag GmbH & Co. KGaA, 2013) pp. 221–244.

[7] T. Nishimatsu, M. Iwamoto, Y. Kawazoe, and U. V. Waghmare, Phys. Rev. B **82**, 134106 (2010).

[8] U. V. Waghmare and K. M. Rabe, Phys. Rev. B **55**, 6161 (1997).

[9] U. V. Waghmare, Accounts of Chemical Research **47**, 3242 (2014).

[10] W. Zhong, D. Vanderbilt, and K. M. Rabe, Phys. Rev. B **52**, 6301 (1995).

[11] D. J. Singh and L. L. Boyer, Ferroelectrics **136**, 95 (1992).

[12] W. Kohn and L. J. Sham, Phys. Rev. **140**, A1133 (1965).

[13] T. Hashimoto, T. Nishimatsu, H. Mizuseki, Y. Kawazoe, A. Sasaki, and Y. Ikeda, Japanese Journal of Applied Physics **43**, 6785 (2004).

[14] D. I. Bilc, R. Orlando, R. Shaltaf, G.-M. Rignanese, J. Íñiguez, and P. Ghosez, Phys. Rev. B **77**, 165107 (2008).

[15] J. P. Perdew, K. Burke, and M. Ernzerhof, Phys. Rev. Lett. **77**, 3865 (1996).

[16] J. P. Perdew, K. Burke, and M. Ernzerhof, Phys. Rev. Lett. **80**, 891 (1998).

[17] Z. Wu and R. E. Cohen, Phys. Rev. B **73**, 235116 (2006).

[18] J. Sun, A. Ruzsinszky, and J. P. Perdew, Phys. Rev. Lett. **115**, 036402 (2015).

[19] J. Sun, R. C. Remsing, Y. Zhang, Z. Sun, A. Ruzsinszky, H. Peng, Z. Yang, A. Paul, U. Waghmare, X. Wu, M. L. Klein, and J. P. Perdew, Nat Chem **8**, 831 (2016).

[20] D. A. Kitchaev, H. Peng, Y. Liu, J. Sun, J. P. Perdew, and G. Ceder, Phys. Rev. B **93**, 045132 (2016).

[21] Z.-H. Yang, H. Peng, J. Sun, and J. P. Perdew, Phys. Rev. B **93**, 205205 (2016).

[22] G. Kresse and J. Furthmüller, Phys. Rev. B **54**, 11169 (1996).

[23] G. Kresse and J. Furthmller, Computational Materials Science **6**, 15 (1996).

[24] G. Kresse and D. Joubert, Phys. Rev. B **59**, 1758 (1999).

[25] T. Nishimatsu, U. V. Waghmare, Y. Kawazoe, and D. Vanderbilt, Phys. Rev. B **78**, 104104 (2008).

[26] “Feram,” `http://loto.sourceforge.net/feram/`.

[27] S. D. Bond, B. J. Leimkuhler, and B. B. Laird, Journal of Computational Physics **151**, 114 (1999).

[28] A. I. Lebedev, Phys. Status Solidi B **249**, 789 (2012).

[29] G. H. Kwei, A. C. Lawson, S. J. L. Billinge, and S. W. Cheong, The Journal of Physical Chemistry **97**, 2368 (1993).

[30] G. Shirane, H. Danner, A. Pavlovic, and R. Pepinsky, Phys. Rev. **93**, 672 (1954).

[31] A. I. Frenkel, F. M. Wang, S. Kelly, R. Ingalls, D. Haskel, E. A. Stern, and Y. Yacoby, Phys. Rev. B **56**, 10869 (1997).

[32] L. F. Wan, T. Nishimatsu, and S. P. Beckman, Journal of Applied Physics **111** (2012).

[33] S. Piskunov, E. Heifets, R. Eglitis, and G. Borstel, Computational Materials Science **29**, 165 (2004).

[34] R. O. Bell and G. Rupprecht, Phys. Rev. **129**, 90 (1963).

[35] Z. Li, M. Grimsditch, C. Foster, and S.-K. Chan, Journal of Physics and Chemistry of Solids **57**, 1433 (1996).

[36] I. Tomeno, Y. Tsunoda, K. Oka, M. Matsuura, and M. Nishi, Phys. Rev. B **80**, 104101 (2009).

[37] K. Ueda, H. Yanagi, R. Noshiro, H. Hosono, and H. Kawazoe, Journal of Physics: Condensed Matter **10**, 3669 (1998).

[38] W. Zhou, H. Deng, P. F, and J. Chu, Applied Physics Letters **105** (2014).

[39] G. Li, T. Kako, D. Wang, Z. Zou, and J. Ye, Journal of Solid State Chemistry **180**, 2845 (2007).

[40] S. Piskunov, A. Gopeyenko, E. Kotomin, Y. Zhukovskii, and D. Ellis, Computational Materials Science **41**, 195 (2007).

[41] R. Eglitis, Solid State Ionics **230**, 43 (2013).

[42] C.-Z. Wang, R. Yu, and H. Krakauer, Phys. Rev. B **54**, 11161 (1996).

[43] R. Wahl, D. Vogtenhuber, and G. Kresse, Phys. Rev. B **78**, 104116 (2008).

[44] O. Dieguez, K. M. Rabe, and D. Vanderbilt, Phys. Rev. B **72**, 144101 (2005).

[45] K. M. Rabe and U. V. Waghmare, Phys. Rev. B **52**, 13236 (1995).

[46] T. Nishimatsu, K. Aoyagi, T. Kiguchi, T. J. Konno, Y. Kawazoe, H. Funakubo, A. Kumar, and U. V. Waghmare, Journal of the Physical Society of Japan **81**, 124702 (2012).

[47] C. J. Johnson, Appl. Phys. Lett. **7**, 221 (1965).

[48] H. Krakauer, R. Yu, C.-Z. Wang, K. M. Rabe, and U. V. Waghmare, Journal of Physics: Condensed Matter **11**, 3779 (1999).

[49] G. Shirane, R. Pepinsky, and B. C. Frazer, Acta Cryst. **9**, 131 (1956).

[50] "Isotropy software suite," `http://iso.byu.edu`.

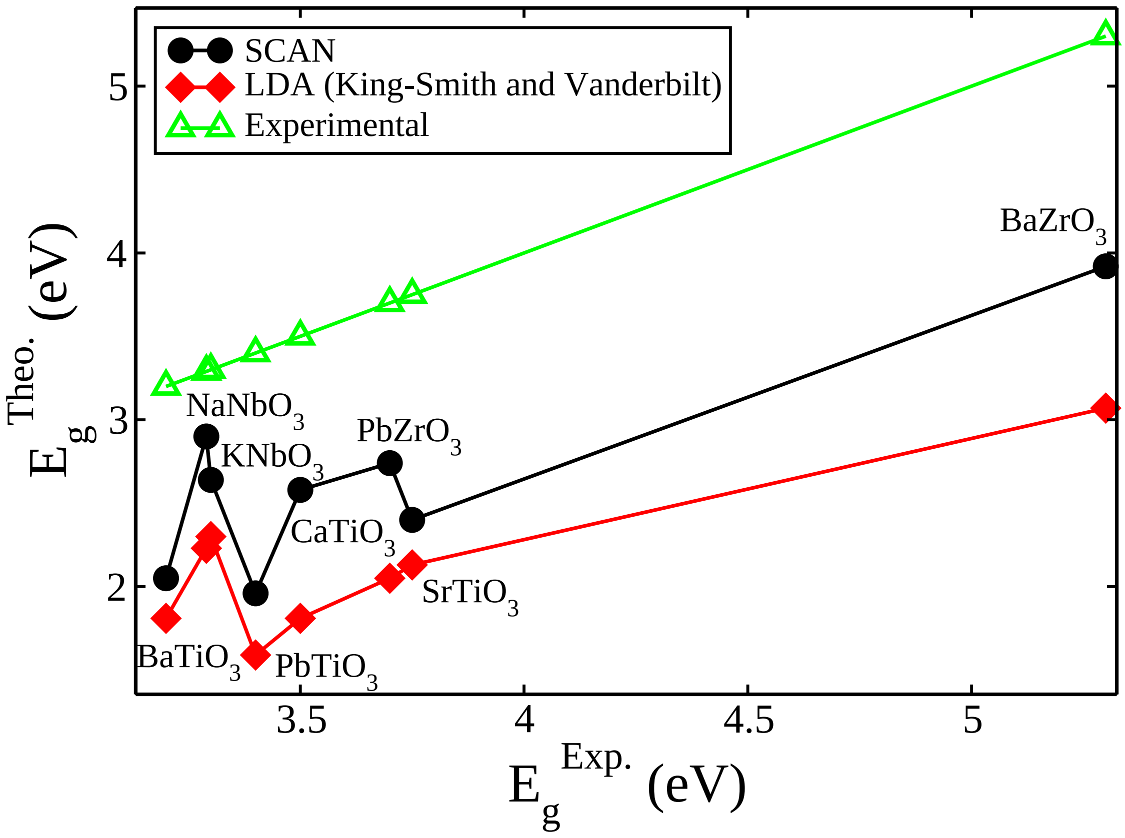

FIG. 1: Optimized lattice constants of eight cubic oxides using the SCAN meta-GGA functional in comparison with experimental and earlier theoretical (using LDA) lattice parameters[4]. Lattice constants (experimental and SCAN metaGGA) of cubic $KNbO_3$ and $BaTiO_3$ are close to each other.

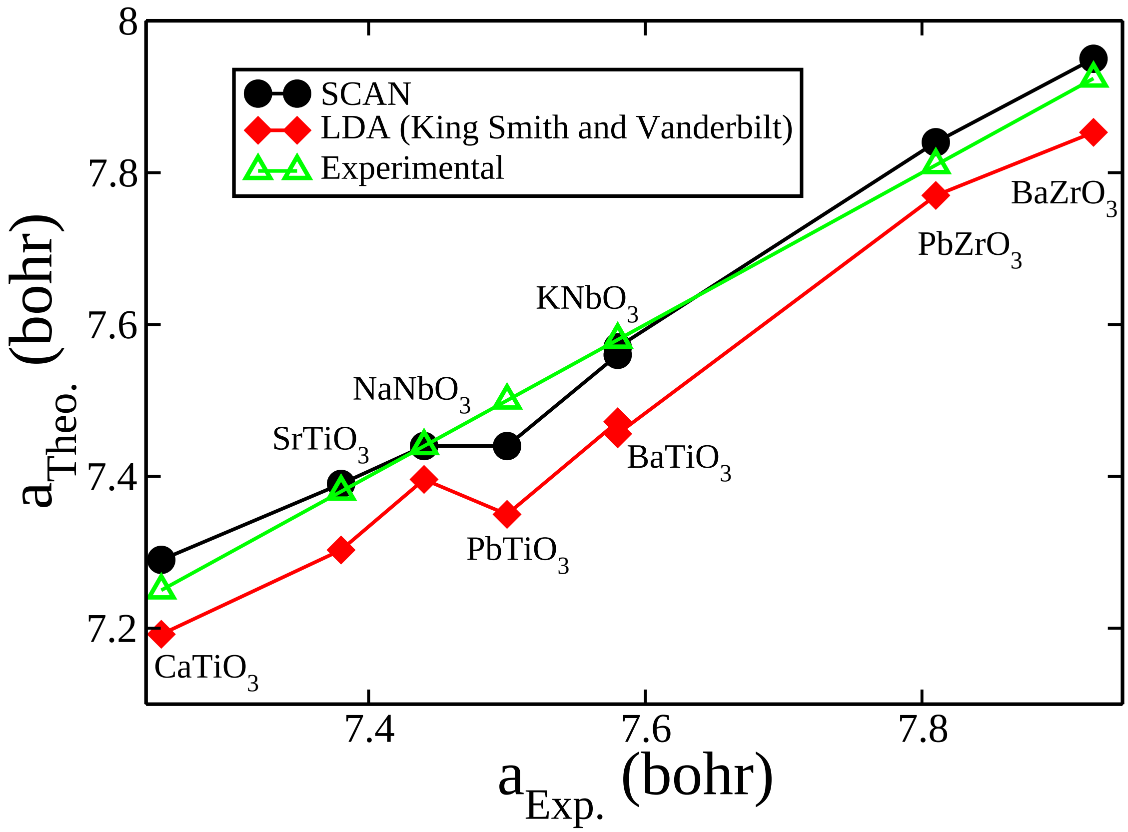

FIG. 2: Direct band gaps of eight perovskites in comparison with earlier theoretical results using LDA[4] and experimentally measured band gaps[33,37–41]. Experimentally measured band gaps of cubic $KNbO_3$ and $NaNbO_3$ are nearly equal.

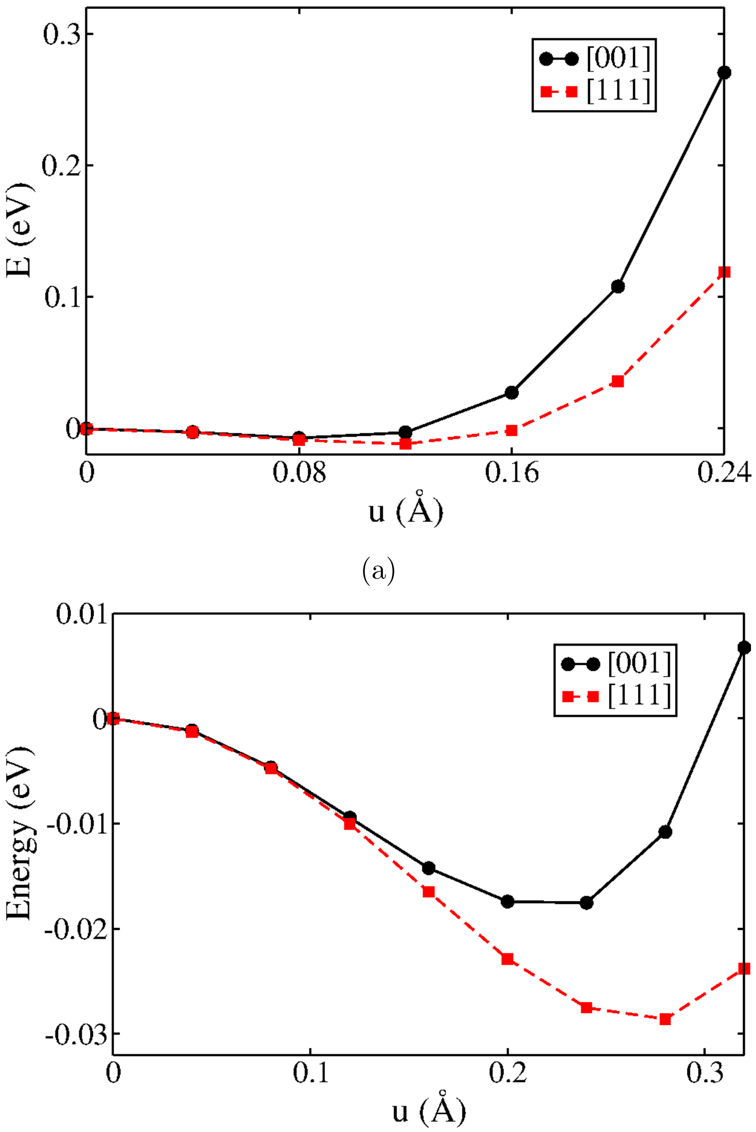

(a)

(b)

FIG. 3: Variations of total energies of unstrained (a) $BaTiO_3$ and (b) $PbTiO_3$ as a function of polar structural distortions (u) along [001] and [111] directions respectively, from SCAN.

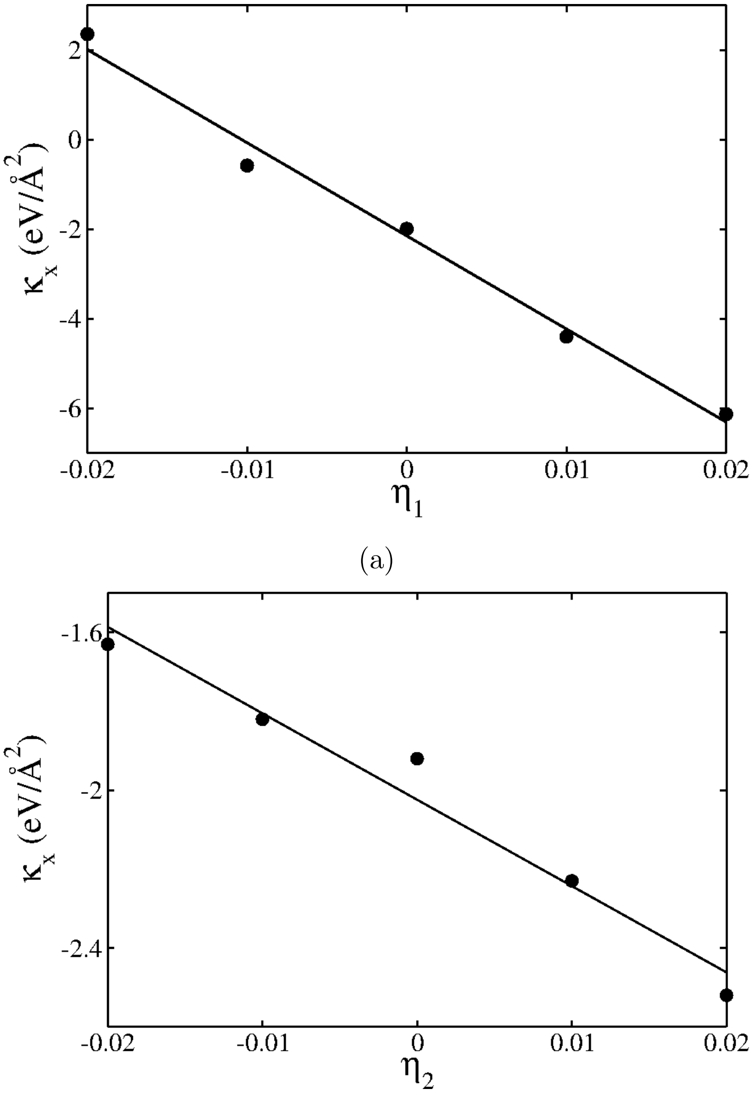

(a)

(b)

FIG. 4: Eigenvalue ($\kappa_x$) of x-polarized soft mode (with $\Gamma_{15}$ symmetry) of $BaTiO_3$ as functions of strains applied (a) along x ($\eta_1$) and (b) y ($\eta_2$) directions, from SCAN.

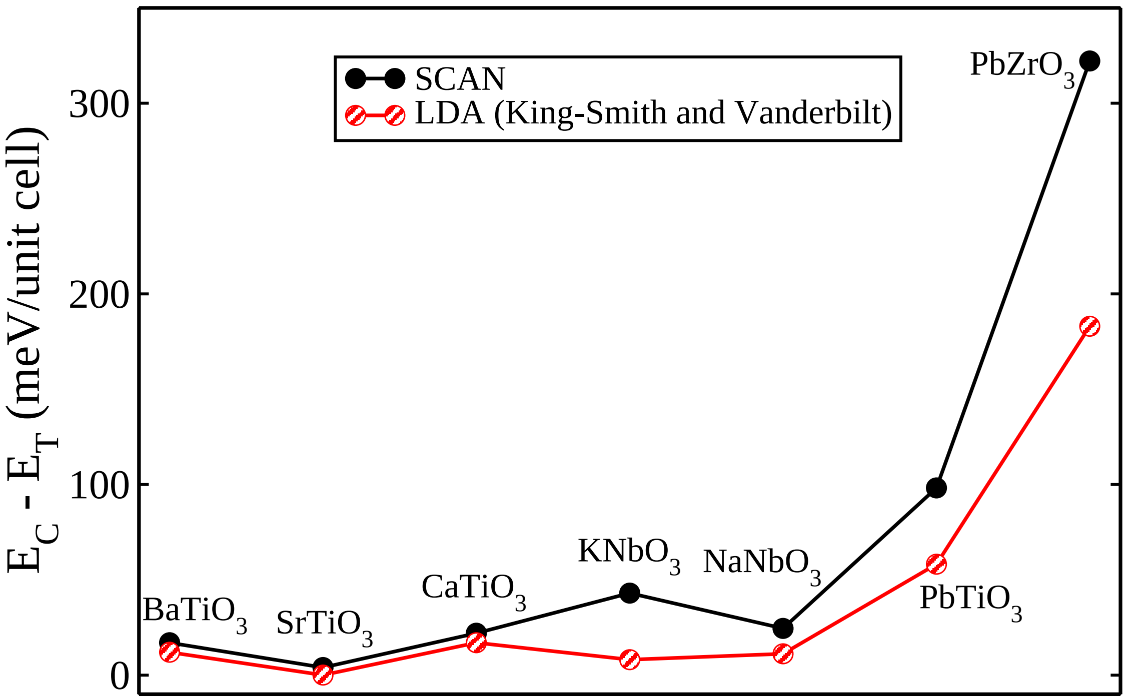

FIG. 5: Calculated energy difference (using fourth-order expansion of energy as a function of soft mode amplitude) between cubic ($E_C$) and tetragonal ($E_T$) phases of perovskites in comparison with earlier theoretical results using LDA[4]. For CaTiO$_3$, we employ the result of another theoretical calculation using LDA from Ref. 44.

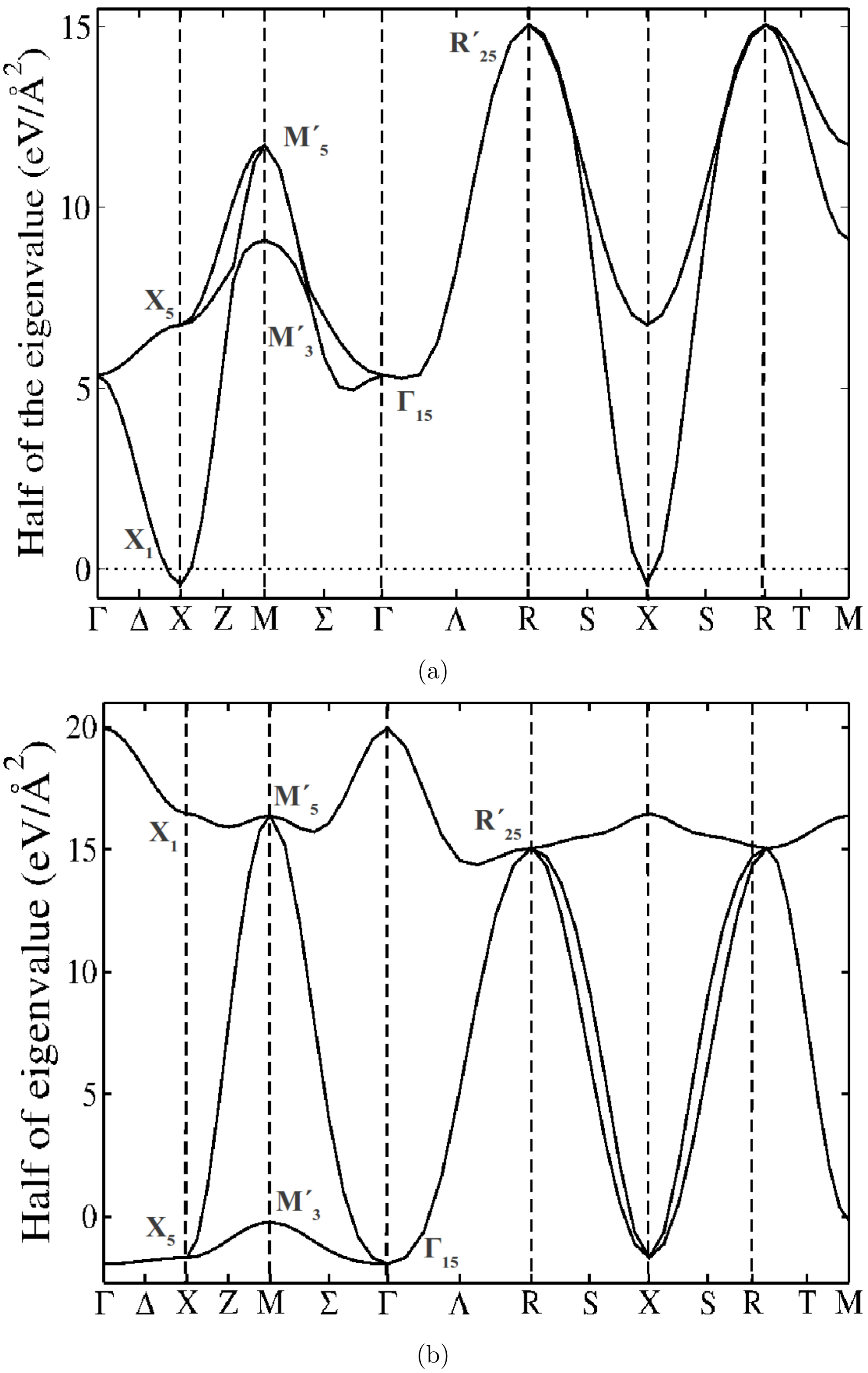

FIG. 6: Half of the eigenvalues of (a) short-range interaction matrix and (b) total (long- and short-range) interaction matrix (Eq. (12) and (13) in Ref. 25) along the high symmetry directions of $BaTiO_3$.

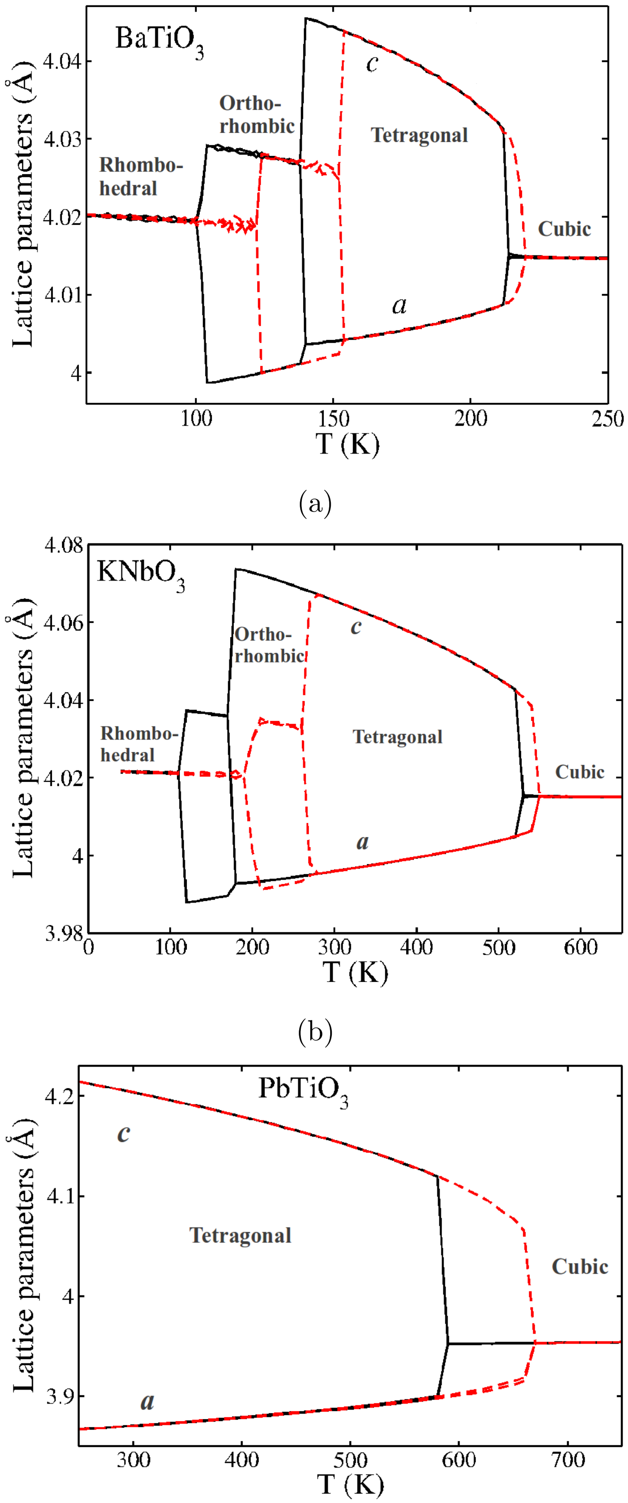

(a)

(b)

(c)

FIG. 7: Simulated temperature dependence of lattice parameters of (a) BaTiO$_3$, (b) KNbO$_3$ and (c) PbTiO$_3$ at zero pressure. Red (dashed) and black (solid) lines represent heating and cooling curves respectively.

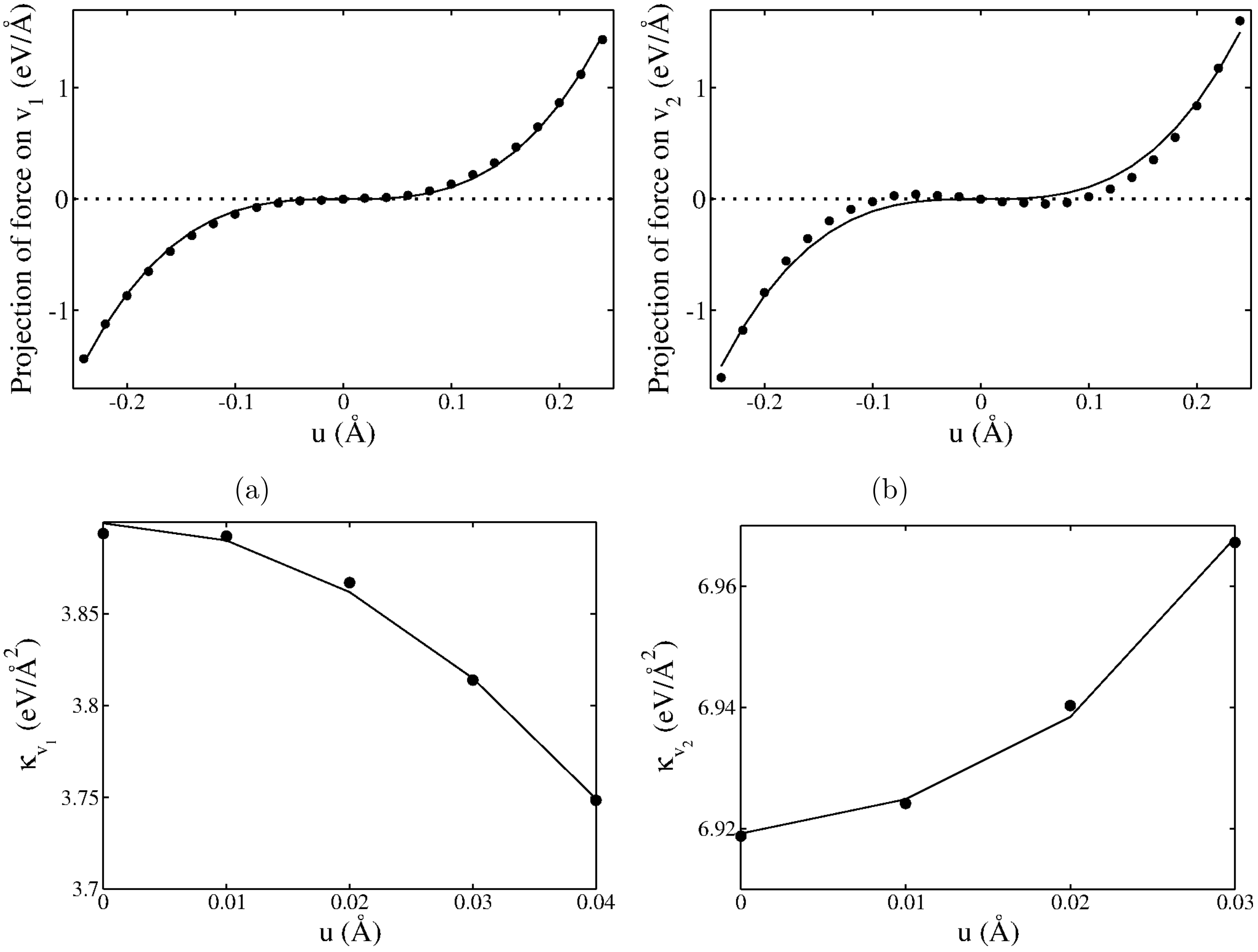

(a) (b)

(c) (d)

FIG. 8: Projection of forces arising due to the freezing of soft mode (a) on $v_1$ and (b) $v_2$ modes of $BaTiO_3$. Eigenvalues of (c) $v_1$ and (d) $v_2$ modes as a function of soft mode amplitude (u).

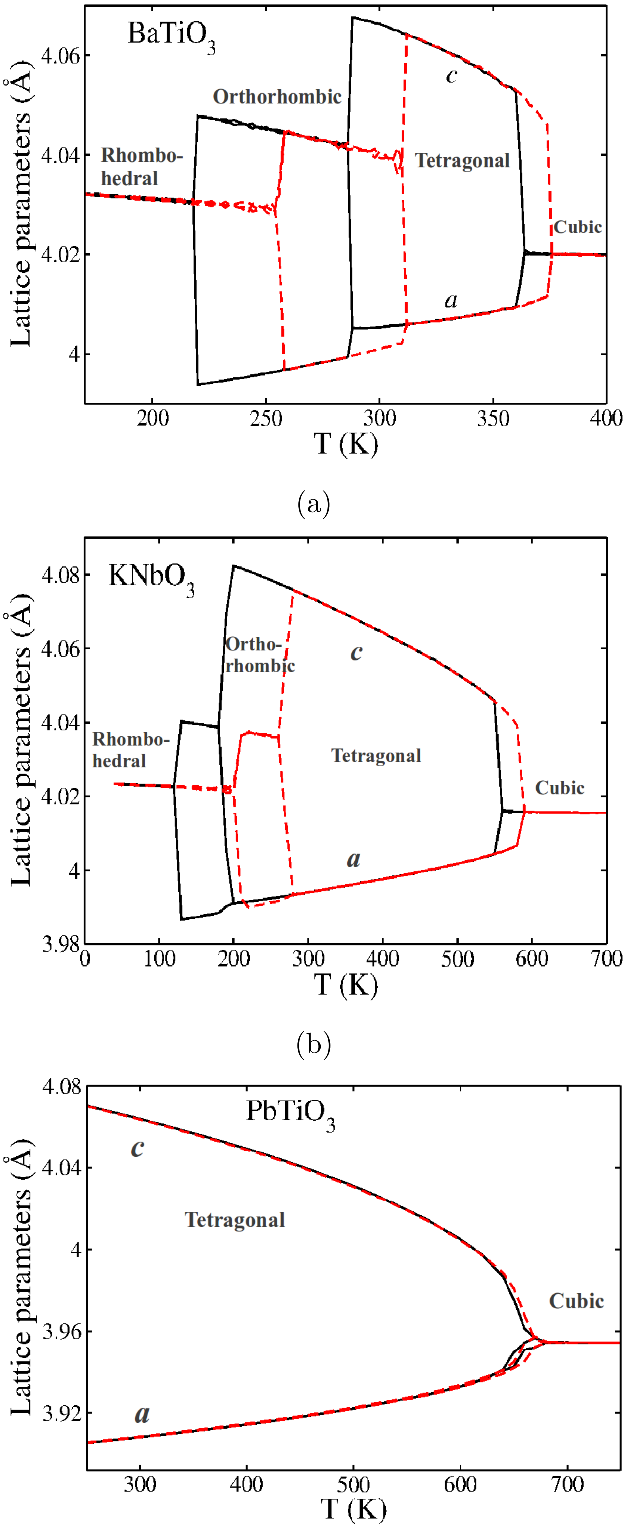

(a)

(b)

(c)

FIG. 9: Estimated $T_C$'s of (a) BaTiO$_3$, (b) KNbO$_3$ and (c) PbTiO$_3$ including the fourth-order coupling between soft and higher energy phonon modes. Heating and cooling curves are indicated by red (dashed) and black (solid) lines respectively.

TABLE I: Optimized tetragonal lattice parameters (in Å) and $z$ component of atomic displacements (from cubic to tetragonal phase) for $BaTiO_3$ and $PbTiO_3$ using the SCAN meta-GGA functional in comparison with earlier theoretical and experimental results[14]. Atomic displacements are given as a fraction of the $c$ parameter.

| Compound | Property | LDA[14] | PBE[14] | WC-GGA[14] | B3LYP[14] | SCAN | Expt.[14] |
|---|---|---|---|---|---|---|---|
| $BaTiO_3$ | $a$ | 3.954 | 4.013 | 3.982 | 3.996 | 3.985 | 3.986 |
| | $\boldsymbol{c/a}$ | 1.006 | 1.035 | 1.012 | 1.066 | 1.027 | 1.010 |
| | $d_z^{Ti}$ | 0.011 | 0.018 | 0.013 | 0.019 | 0.016 | 0.015 |
| | $d_z^{O_I}$ | -0.014 | -0.039 | -0.022 | -0.057 | -0.029 | -0.023 |
| | $d_Z^{O_{II}}$ | -0.009 | -0.022 | -0.013 | -0.031 | -0.017 | -0.014 |
| $PbTiO_3$ | $a$ | 3.872 | 3.834 | 3.870 | 3.819 | 3.881 | 3.88 |
| | $\boldsymbol{c/a}$ | 1.041 | 1.221 | 1.086 | 1.277 | 1.110 | 1.063 (300 K) |
| | $d_z^{Ti}$ | 0.037 | 0.062 | 0.044 | 0.076 | 0.029 | 0.040 |
| | $d_z^{O_I}$ | 0.090 | 0.189 | 0.121 | 0.223 | 0.118 | 0.112 |
| | $d_Z^{O_{II}}$ | 0.106 | 0.178 | 0.133 | 0.198 | 0.120 | 0.112 |

TABLE II: Optimized lattice parameters of orthorhombic and rhombohedral phases of $BaTiO_3$ and $KNbO_3$ using the SCAN meta-GGA functional in comparison with earlier theoretical and experimental results[29–32].

| Compound | Phase | Lattice parameters | PBE-GGA | WC-GGA[32] | SCAN | Expt.[29–31] |
|---|---|---|---|---|---|---|
| $BaTiO_3$ | Rhombo | $a$ (Å) | 4.073 | | 4.029 | 4.003 |
| | | $\alpha$ (°) | 89.76 | | 89.83 | 89.84 |
| | Ortho | $a$ (Å) | 4.110 | | 4.047 | 4.041 |
| | | $b$ (Å) | 3.996 | | 3.983 | 3.982 |
| | | $c$ (Å) | 4.113 | | 4.051 | 4.065 |
| $KNbO_3$ | Rhombo | $a$ (Å) | 4.071 | 4.041 | 4.032 | 4.016 |
| | | $\alpha$ (°) | 89.81 | 89.85 | 89.82 | 89.83 |
| | Ortho | $a$ (Å) | 4.111 | 4.141 | 4.055 | 4.080 |
| | | $b$ (Å) | 3.988 | 3.980 | 3.969 | 3.973 |
| | | $c$ (Å) | 4.119 | 4.179 | 4.057 | 4.116 |

TABLE III: Elastic constants (in GPa) of cubic perovskites using the SCAN meta-GGA functional in comparison with earlier theoretically-calculated values using LDA[4] and experimentally-measured values[33,36].

| | | Method | | |
|---|---|---|---|---|
| Compound | Elastic constant | SCAN | LDA[4] | Expt.[33,36] |
| $BaTiO_3$ | $C_{11}$ | 328 | 329 | 206 |
| | $C_{12}$ | 118 | 117 | 140 |
| | $C_{44}$ | 131 | 130 | 126 |
| $SrTiO_3$ | $C_{11}$ | 374 | 389 | 316 |
| | $C_{12}$ | 113 | 105 | 101 |
| | $C_{44}$ | 120 | 155 | 119 |
| $CaTiO_3$ | $C_{11}$ | 399 | 407 | |
| | $C_{12}$ | 110 | 96 | |
| | $C_{44}$ | 104 | 102 | |
| $PbTiO_3$ | $C_{11}$ | 340 | 335 | 229 |
| | $C_{12}$ | 135 | 146 | 101 |
| | $C_{44}$ | 108 | 100 | 100 |
| $KNbO_3$ | $C_{11}$ | 427 | 465 | 232 |
| | $C_{12}$ | 83 | 67 | 90 |
| | $C_{44}$ | 103 | 96 | 75 |
| $NaNbO_3$ | $C_{11}$ | 472 | 482 | 230 |
| | $C_{12}$ | 84 | 70 | 90 |
| | $C_{44}$ | 77 | 78 | 76 |
| $PbZrO_3$ | $C_{11}$ | 332 | 371 | |
| | $C_{12}$ | 94 | 86 | |
| | $C_{44}$ | 67 | 67 | |
| $BaZrO_3$ | $C_{11}$ | 325 | 335 | |
| | $C_{12}$ | 88 | 95 | |
| | $C_{44}$ | 93 | 89 | |

TABLE IV: Predicted zone-centre optical phonon frequencies (in cm$^{-1}$) of BaTiO$_3$, PbTiO$_3$, SrTiO$_3$ and KNbO$_3$ at theoretical lattice constants in comparison with earlier theoretically-calculated and experimentally-measured frequencies[14,42,43].

| | | Functional | | | | | | | |
|---|---|---|---|---|---|---|---|---|---|
| Compound | Symmetry | LDA[14,43] | WC-GGA[14] | B1-WC[14] | PBE[43] | HSE[43] | LDA-LAPW[42] | SCAN | Exp.[14,42,43] |
| BaTiO$_3$ | $\Gamma_{15}$ (TO1) | 75i | 128i | 145i | | | | 196i | |
| | $\Gamma_{15}$ (TO2) | 193 | 186 | 195 | | | | 182 | 182 |
| | $\Gamma_{15}$ (TO3) | 480 | 469 | 482 | | | | 478 | 482 |
| | $\Gamma_{25}$ (TO4) | 286 | 282 | 299 | | | | 297 | 306 |
| PbTiO$_3$ | $\Gamma_{15}$ (TO1) | 127i | 132i | 146i | | | | 147i | |
| | $\Gamma_{15}$ (TO2) | 145 | 141 | 138 | | | | 140 | |
| | $\Gamma_{15}$ (TO3) | 515 | 510 | 513 | | | | 530 | |
| | $\Gamma_{25}$ (TO4) | 219 | 211 | 231 | | | | 227 | |
| SrTiO$_3$ | $\Gamma_{15}$ (TO1) | 80 | | | 115i | 74i | | 86 | 91 (297 K) |
| | $\Gamma_{15}$ (TO2) | 177 | | | 147 | 162 | | 173 | 169 (297 K) |
| | $\Gamma_{15}$ (TO3) | 563 | | | 512 | 533 | | 553 | 544 (297 K) |
| | $\Gamma_{25}$ (TO4) | 226 | | | 234 | 250 | | 244 | 265 (297 K) |
| KNbO$_3$ | $\Gamma_{15}$ (TO1) | 143i | | | | | 197i | 247i | |
| | $\Gamma_{15}$ (TO2) | 188 | | | | | 170 | 207 | 198 |
| | $\Gamma_{15}$ (TO3) | 506 | | | | | 473 | 483 | 521 |
| | $\Gamma_{25}$ (TO4) | | | | | | 243 | 272 | 280 |

TABLE V: Harmonic ($\kappa$ in eV/Å$^2$), anharmonic ($\alpha$ and $\gamma$ in eV/Å$^4$) and strain-phonon coupling parameters (B$_{1xx}$, B$_{1yy}$ and B$_{4yz}$ in eV/Å$^2$) in comparison with earlier theoretically-calculated values using LDA[4]. $\kappa$ is the harmonic and $\alpha$ and $\gamma$ are the anharmonic coupling coefficients (estimated by fitting the fourth-order polynomial in soft mode amplitude) in the on-site energy.

| | | Coupling coefficients | | | | | | | |
|---|---|---|---|---|---|---|---|---|---|
| Compound | Functional | $\kappa$ | $\alpha$ | $\gamma$ | B$_{1xx}$ | B$_{1yy}$ | B$_{4yz}$ | $\alpha'$ | $\gamma'$ |
| BaTiO$_3$ | SCAN | -1.92 | 112.73 | -158.93 | -225.76 | -18.04 | -20.93 | 57.92 | -36.54 |
| | LDA[4] | -1.68 | 110.32 | -163.07 | -210.32 | -19.29 | -7.72 | 60.68 | -42.75 |
| SrTiO$_3$ | SCAN | 0.49 | 21.37 | -22.06 | -64.64 | -39.94 | 46.41 | 16.89 | -44.47 |
| | LDA[4] | -0.086 | 51.72 | -65.85 | -136.04 | 5.78 | -10.61 | 32.06 | -3.45 |
| CaTiO$_3$ | SCAN | -0.47 | 4.14 | 1.89 | -49.97 | -30.01 | -10.81 | 2.59 | 2.52 |
| | LDA[4] | -1.11 | 7.93 | -2.07 | -56.92 | 5.78 | -9.65 | 4.48 | 21.03 |
| PbTiO$_3$ | SCAN | -0.77 | 6.79 | -4.41 | -66.37 | -2.99 | -23.25 | 1.59 | 1.79 |
| | LDA[4] | -1.24 | 15.17 | -15.51 | -75.25 | 0.00 | -2.89 | 7.58 | 8.62 |
| KNbO$_3$ | SCAN | -3.14 | 110.67 | -149.97 | -257.21 | 15.53 | -3.28 | 57.58 | -14.82 |
| | LDA[4] | -1.49 | 130.32 | -211.34 | -290.40 | 31.84 | -0.96 | 63.43 | -38.27 |
| NaNbO$_3$ | SCAN | -1.53 | 28.27 | -31.37 | 29.14 | -44.96 | 6.66 | 24.82 | -22.07 |
| | LDA[4] | -1.19 | 57.92 | -88.26 | -164.98 | 48.24 | 0.00 | 32.06 | -14.14 |
| PbZrO$_3$ | SCAN | -1.36 | 2.41 | -0.17 | 33.67 | 5.49 | -18.52 | 1.45 | -3.75 |
| | LDA[4] | -1.51 | 3.79 | -4.48 | -21.22 | 6.75 | -0.96 | 3.10 | -1.03 |
| BaZrO$_3$ | SCAN | 1.82 | 1.69 | 2.41 | 16.98 | 29.62 | 19.39 | 0.55 | -1.52 |
| | LDA[4] | 0.75 | 5.52 | 0.00 | -45.34 | 6.75 | -10.61 | 3.10 | 18.62 |

TABLE VI: Computed eigenvectors ($\xi_z^{atom}$ (unitless)) and amplitudes of the soft modes of eight perovskites in comparison with earlier LDA results.[4,44]

| Compound | Method | $\xi_z^A$ | $\xi_z^B$ | $\xi_z^{O_{1,2}}$ | $\xi_z^{O_3}$ | Amplitude (bohr) |
|---|---|---|---|---|---|---|
| $BaTiO_3$ | SCAN | 0.15 | 0.77 | -0.18 | -0.56 | 0.24 |
| | LDA[4] | 0.20 | 0.76 | -0.21 | -0.53 | 0.25 |
| $PbTiO_3$ | SCAN | 0.65 | 0.43 | -0.40 | -0.27 | 0.56 |
| | LDA[4] | 0.57 | 0.51 | -0.41 | -0.27 | 0.54 |
| $KNbO_3$ | SCAN | 0.12 | 0.80 | -0.21 | -0.50 | 0.30 |
| | LDA[4] | 0.18 | 0.80 | -0.31 | -0.37 | 0.22 |
| $SrTiO_3$ | SCAN | 0.52 | 0.57 | -0.39 | -0.30 | 0.0 |
| | LDA[44] | 0.49 | 0.60 | -0.41 | -0.27 | |
| $CaTiO_3$ | SCAN | 0.74 | 0.27 | -0.42 | 0.17 | 0.38 |
| | LDA[44] | 0.68 | 0.36 | -0.44 | -0.17 | |
| $NaNbO_3$ | SCAN | 0.35 | 0.70 | -0.38 | -0.31 | 0.38 |
| | LDA[44] | 0.43 | 0.64 | -0.43 | -0.21 | |
| $PbZrO_3$ | SCAN | 0.81 | 0.09 | -0.41 | -0.09 | 1.06 |
| | LDA[44] | 0.77 | 0.15 | -0.44 | -0.04 | |
| $BaZrO_3$ | SCAN | 0.75 | 0.23 | -0.43 | -0.13 | 0.0 |
| | LDA[44] | 0.70 | 0.27 | -0.46 | -0.05 | |

TABLE VII: Calculated local and short-range interaction parameters (in eV/Å$^2$) of $BaTiO_3$, $PbTiO_3$ and $KNbO_3$ in comparison with earlier theoretical results determined using LDA[7,8,46] and WC-GGA functionals[7,26].

| Compound | parameter | SCAN | LDA[7,8,46] | WC-GGA[7,26] |
|---|---|---|---|---|
| $BaTiO_3$ | $\kappa_2$ | 8.31 | 5.52 | 8.53 |
| | $j_1$ | -2.54 | -2.65 | -2.08 |
| | $j_2$ | -0.82 | 3.906 | -1.12 |
| | $j_3$ | 0.78 | 0.90 | 0.68 |
| | $j_4$ | -0.52 | -0.79 | -0.61 |
| | $j_5$ | 0.0 | 0.56 | 0.0 |
| | $j_6$ | 0.32 | 0.36 | 0.27 |
| | $j_7$ | 0.0 | 0.18 | 0.0 |
| $PbTiO_3$ | $\kappa_2$ | 1.36 | 1.17 | |
| | $j_1$ | -1.36 | 1.17 | |
| | $j_2$ | 4.84 | -1.35 | |
| | $j_3$ | 0.45 | 4.98 | |
| | $j_4$ | -0.11 | 0.22 | |
| | $j_5$ | 0.60 | -0.018 | |
| | $j_6$ | -0.09 | -0.083 | |
| | $j_7$ | -0.05 | -0.204 | |
| $KNbO_3$ | $\kappa_2$ | 10.06 | | 11.42 |
| | $j_1$ | -5.06 | | -3.27 |
| | $j_2$ | 1.87 | | -1.15 |
| | $j_3$ | 1.09 | | 1.10 |
| | $j_4$ | 0.07 | | -0.66 |
| | $j_5$ | 0.0 | | 0.0 |
| | $j_6$ | 0.43 | | 0.30 |
| | $j_7$ | 0.0 | | 0.0 |

TABLE VIII: Estimated $T_c$'s of $BaTiO_3$, $PbTiO_3$ and $KNbO_3$ in comparison with earlier theoretical[7,8,46] and experimental $T_C$'s[26,42,47–49].

| Compound | exchange-correlation functional | R↔O | O↔T | T↔C |
|---|---|---|---|---|
| $BaTiO_3$ | SCAN | 111 K | 141 K | 213 K |
| | SCAN (including anharmonic coupling between phonons) | 230 K | 278 K | 375 K |
| | LDA, 0.0 GPa[7] | 95 K | 110 K | 137 K |
| | LDA, -5.0 GPa[7] | 210 K | 245 K | 320 K |
| | WC-GGA, 0.0 GPa[7] | 102 K | 160 K | 288 K |
| | WC-GGA, -2.0 GPa[7] | 117 K | 218 K | 408 K |
| | WC-GGA, -0.005T GPa[7] | 103 K | 187 K | 411 K |
| | Exp.[47] | 183 K | 278 K | 403 K |
| $KNbO_3$ | SCAN | 160 K | 225 K | 540 K |
| | SCAN (including anharmonic coupling between phonons) | 160 K | 230 K | 565 K |
| | LDA (experimental lattice constant)[48] | 210 K | 260 K | 370 K |
| | WC-GGA[26], 0.0 GPa | 177 K | 310 K | 660 K |
| | WC-GGA[26], -0.001T GPa | 175 K | 323 K | 703 K |
| | Exp.[42] | 210 K | 488 K | 701 K |
| $PbTiO_3$ | SCAN | | | 630 K |
| | SCAN (including anharmonic coupling between phonons) | | | 675 K |
| | LDA (experimental lattice constant)[8,46] | | | 635 K |
| | Exp.[49] | | | 763 K |